Reviews in Mathematical Physics

The application of numerical topological invariants in simulations of knotted rings: A comprehensive Monte Carlo approach

Franco Ferrari

CASA* and Institute of Physics, University of Szczecin,
Wielkopolska 15, 70-451 Szczecin, Poland
franco@feynman.fiz.univ.szczecin.pl

Yani Zhao

Max Planck Institute for Polymer Research,
Ackermannweg 10, 55128 Mainz, Germany
zhaoyani@mpip-mainz.mpg.de

Received (Day Month Year)
Revised (Day Month Year)

In this work a general Monte Carlo framework is proposed for applying numerical knot invariants in simulations of systems containing knotted one-dimensional ring-shaped objects like polymers and vortex lines in fluids, superfluids or other quantum liquids. A general prescription for smoothing the sharp corners appearing in discrete knots consisting of segments joined together is provided. Smoothing is very important for the correct evaluation of numerical knot invariants.

A discrete version of framing is adopted in order to eliminate singularities that are possibly arising when computing the invariants. The presented algorithms for smoothing, eliminating potentially dangerous singularities and speeding up the calculations are quite general and can be applied to any discrete knot defined off or on-lattice.

This is one of the first attempts to use numerical knot invariants in order to avoid potential topology breakings during the sampling process taking place in computer simulations, in which millions of knot conformations are randomly generated. As an application, the energy domain of knotted polymers rings subjected to short-range interactions is studied using the so-called Vassiliev knot invariant of degree 2.

Keywords: Statistical mechanics, structure of matter; finite type and quantum invariants, topological quantum field theories (TQFT); Monte Carlo methods.

Mathematics Subject Classification 2000: 82-XX, 57K16, 65C05

1. Introduction

There are many situations in which it is necessary to distinguish the topological properties of ring-shaped quasi one-dimensional objects. This is for instance the case of polymers [1,2], vortex structures in nematic liquid crystals [3] or ^3He superfluid [4,5] and disclination lines in chiral nematic colloids [6,7,8]. In order to ascertain the type of a knot, it is possible to apply the so-called knot invariants.

These mathematical quantities, which remain unchanged under ambient isotopy, are usually represented in the form of polynomials, like for example the Alexander [9], Kauffman [10] or the HOMFLY polynomials [11]. Alternatively, certain knot invariants may be defined in terms of multiple curvilinear integrals, in which the integrations are performed along the loop formed by the knot in space or elements of it [12,13,14,15,16,17]. The latter invariants belong to the family of the so-called numerical invariants and are not limited only to knots, as there exist also numerical invariants for links. They may be derived from the Wilson loop amplitudes of topological field theories [16,17].

Particularly important for applications is the case in which knots (or links) are constructed by joining together at their ends a set of N segments. Discrete knots of this kind are in fact the most common concrete realizations of knots in numerical simulations. Formally, a discrete knot is a C^0-curve, i. e. a curve that is piecewise smooth and is characterized by sharp corners at the joints between contiguous segments. While there exist already well established mathematical algorithms in order to compute numerically polynomial knot invariants, see for instance the pioneering work [18], there are not many studies concerning the numerical computation of knot invariants given in the form of multiple line integrals for such discrete knots. This works aims to fill this gap. Of course, the calculation of line integrals over discrete data is a textbook subject [19,20]. Moreover, problems in which knots are discretized using splines have been investigated for example in [21]. However, we are facing here a somewhat different problem that is specific to the calculation of knot invariants expressed as multiple curvilinear integrals in computer simulations. Such invariants turn out to be not well defined in the case of discrete knots. As we show in this paper, any attempt to compute the exact value of an invariant like the Vassiliev knot invariant of degree 2 fails. The reason of this failure is due to the presence of the non-smooth corners at the joints between contiguous segments. One of the main goals of this work is to solve this difficulty by replacing the piecewise smooth curve representing a discrete knot with a more regular one. Several techniques for smoothing curves are already available, see for example Refs. [22,23] and [24,25,26], but a dedicated fast algorithm for smoothing discrete knots that is suitable for numerical simulations in which millions of different knot conformations are sampled is still missing.

In order to provide a smoothing procedure that is sufficiently fast and is valid for any discrete knot without destroying its topology, the following strategy has been adopted. First, it is determined a region around each sharp corner that is free from other elements of the knot apart from the two contiguous segments that have their joint at that corner. This task is relatively simple on a lattice, but not off-lattice or whenever the segments composing a knot are allowed to get arbitrarily close to each other. We develop here a technique that is valid in the most general case. The idea is to surround each sharp corner with a sphere. The radii of these spheres are chosen in such a way that different spheres do not overlap. Next, we replace the sharp corners with a special family of arcs of smooth curves. These arcs

are constructed in such a way that they lie entirely inside the spheres. We show that the proposed procedure transforms the original discrete loops into G^1-curves[a] without altering their topological configurations. This is sufficient to determine the topological type of the smoothed knot using numerical knot invariants, a task that is crucial in computer simulations of polymers rings with non-trivial topology. In fact, during the sampling process, the conformations of a discrete knot are randomly changed very fast and it is important to check that the topology of the knot is preserved after each change, see for instance Ref. [29] on that point. We provide here a comprehensive Monte Carlo approach for the computation of the value of general numerical topological invariants. The time necessary to evaluate the several multiple curvilinear integrals appearing in the expressions of these invariants is considerably reduced by adopting several speeding up tricks. Together with the addition of an high degree of parallelisation and the use of GPUs, the detection of the type of a knot via numerical invariants becomes competitive with respect to polynomial invariants. Indeed, already the calculation of a relatively simple polynomial invariant like that of Alexander requires that the knot is projected onto a plane and all the crossing points in which the lines of the projected knot intersect themselves must be inspected. The expression of the Alexander polynomial for a given knot is then obtained by computing the determinant of a matrix of dimension $\mathcal{M}\times\mathcal{M}$, where $\mathcal{M}$ is the number of crossings. In a tight knot $\mathcal{M}$ can grow very large as it is well illustrated by Fig. 1, in which a knot composed by 3994 segments on a cubic lattice is represented. With the provided algorithms, numerical invariants become a valid alternative.

As an application, we search for conformations of minimal energy in the concrete case of knots formed by polymers whose monomers are subjected to very short-range attractive interactions. This is a computationally demanding problem in the case of long polymers because billions of conformations have to be explored in a reasonable time while keeping the topology of the knot fixed. To detect possible topology changes during the sampling, we use the Vassiliev knot invariant of degree 2 of a knot C [28], denoted here $\varrho(C)$. The main advantages of choosing this numerical invariant are its relative simplicity and the fact that its exact values for different knot types are known. This makes easier to test the correctedness of numerical results. With the smoothing procedure and the Monte Carlo approach proposed in this work, $\varrho(C)$ may be calculated numerically with an arbitrarily high precision. We stress the fact that while all knots treated in our polymer simulations are originally defined on a simple cubic lattice, this is no longer true after the transformations made in order to speed up the calculations. In particular, this is due to an algorithm that has been provided in order to reduce by a factor three the number of segments without changing the topology of a knot.

In order to derive the Vassiliev invariant of degree 2, the evaluation of compli-

[a]We recall that a G^1-curve is a tangent vector geometrically continuous curve characterized by the fact that the unit tangent vector to the curve is continuous [27].

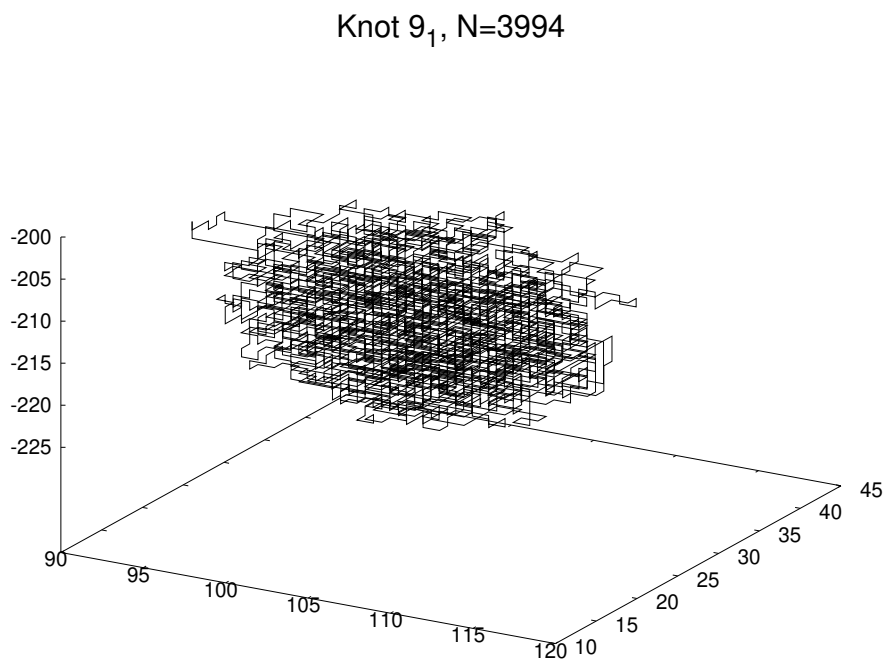

Fig. 1. A knot 9_1 composed by $N = 3994$ segments in a cubic lattice. The knot is compressed in a volume of $30 \times 30 \times 30$ lattice units.

cated quadruple and triple line integrals is required. In this case, the Monte Carlo integration scheme adopted in this work is more suitable than traditional integration methods [30]. To randomly transform the knots, the pivot moves have been exploited [31], but there are several other valid alternatives like the pull moves [32] and the BFACF moves [33,34]. Our sampling strategy consists in a applying successively random transformations starting from a seed C_0. In this way, a set of loops $C_1, C_2, \ldots, C_i, \ldots$ is generated. In order to prevent unwanted changes of topology in passing from C_i to C_{i+1}, it is shown here that is much more convenient to compute the difference $\varrho(C_{i+1}) - \varrho(C_i)$ rather then evaluating $\varrho(C_i)$ and $\varrho(C_{i+1})$ separately. The reason is that the whole information about the topology of C_i and C_{i+1} is not necessary if we only wish to assess possible topological differences between two knots of which one of them has been obtained after a random change of a portion of the other. To this purpose it is just sufficient to know if the quantity $\varrho(C_{i+1}) - \varrho(C_i)$ is equal to zero or not.

The material presented in this paper is divided as follows. In the next Section the Vassiliev invariant of degree 2 is defined in the case of general smooth curves. This invariant will be used throughout this work as a case study. In Section 3 a suit-

able discretization scheme is provided for knots that are represented as piecewise smooth curves parametrized by a continuous variable $S \in [0, N]$. Next, a Monte Carlo based formula for computing numerical knot invariants is introduced. In order to regularize singularities that are possibly arising in some of the terms to be integrated, a numerical version of the so-called framing [35] procedure is implemented. Section 4 starts with a simple example showing that the calculation of numerical topological invariants does not converge to the exact result in the case of a discrete knot. To avoid this problem, a smoothing algorithm is provided in order to transform a general discrete knot into a G^1-curve. This algorithm is very fast and works well on various kinds of lattices. Yet, there are situations, for instance in off-lattice calculations, in which the topology of the knot can turn out to get modified after smoothing. For that reason, in Section 5 the smoothing algorithm is extended to ensure the preservation of topology in the most general case. The values of $\varrho(C)$ before and after smoothing are numerically computed for knots originally defined on a lattice and compared with the exact results. We show that, after smoothing, the Vassiliev invariant of degree 2 can be evaluated with an arbitrary precision. This is not true in the case of discrete knots. We find that the departure from the exact value of $\varrho(C)$ is roughly proportional to the number of sharp corners that are present in the conformation of the discrete knot. In Section 6 methods for speeding up the calculations of numerical knot invariants are discussed. In particular, an algorithm that enables to decrease considerably the number of segments contained in a discrete knots is developed. Section 7 presents a practical application of the above findings, namely the search of rare, ultra-low energy configurations of a knot formed by a polymer ring fluctuating in a bad solution. Finally, the Conclusions are drawn in Section 8.

2. The Vassiliev invariant of degree 2

Let us consider a general knot of length L in the flat three dimensional space $\mathbb{R}^3$ spanned by a set of cartesian coordinates $\boldsymbol{x} = (x^1, x^2, x^3)$. The space indices are labeled with greek letters $\mu, \nu, \rho, \ldots = 1, 2, 3$. The Alexander-Briggs notation for denoting knots is used. In this Section, the spatial loop C formed in the space by the knot is chosen to be a smooth curve $\boldsymbol{x}(s) : [0, L] \longrightarrow \mathbb{R}^3$ parametrized using its arc-length $0 \leq s \leq L$. Different points on the curve corresponding to different values of the arc-length s, t, u and v will be denoted with the symbols $x^\mu(s), y^\nu(t), z^\rho(u)$ and $w^\sigma(v)$, with $\mu, \nu, \rho, \sigma = 1, 2, 3$. As a convention, summation over repeated indices is understood. Moreover, let $\dot{x}^\mu(s)$ be the derivative of $x^\mu(s)$ with respect to s. An analogous notation holds for $\dot{y}^\nu(t), \dot{z}^\rho(u)$ and $\dot{w}^\sigma(v)$. Finally, $\epsilon_{\mu\nu\rho}$ is the completely antisymmetric tensor uniquely defined by the condition $\epsilon_{123} = 1$.

With the above settings, the Vassiliev knot invariant of degree 2 $\varrho(C)$ of a knot C can be written as follows [15,16,36]:

$$\varrho(C) = \varrho_1(C) + \varrho_2(C) \tag{2.1}$$

where $\varrho_1(C)$ and $\varrho_2(C)$ are two path ordered multiple line integrals given by:

$$\varrho_1(C) = \int_0^L ds \int_0^s dt \int_0^t du F_1(\boldsymbol{x}(s), \boldsymbol{y}(t), \boldsymbol{z}(u); \dot{\boldsymbol{x}}(s), \dot{\boldsymbol{y}}(t), \dot{\boldsymbol{z}}(u)) \tag{2.2}$$

and

$$\varrho_2(C) = \int_0^L ds \int_0^s dt \int_0^t du \int_0^u dv F_2(\boldsymbol{x}(s), \boldsymbol{y}(t), \boldsymbol{z}(u), \boldsymbol{w}(v); \dot{\boldsymbol{x}}(s), \dot{\boldsymbol{y}}(t), \dot{\boldsymbol{z}}(u), \dot{\boldsymbol{w}}(v)) \tag{2.3}$$

The quantities F_1 and F_2 are defined below:

$$\begin{aligned} -32\pi^3 F_1(\boldsymbol{x}, \boldsymbol{y}, \boldsymbol{z}; \dot{\boldsymbol{x}}, \dot{\boldsymbol{y}}, \dot{\boldsymbol{z}}) &= C_1 C_2 C_3 \left[\dot{\boldsymbol{y}} \cdot \dot{\boldsymbol{z}} (\dot{\boldsymbol{x}} \cdot \boldsymbol{c}) + \dot{\boldsymbol{x}} \cdot \dot{\boldsymbol{z}} (\dot{\boldsymbol{y}} \cdot \boldsymbol{b}) - \dot{\boldsymbol{x}} \cdot \dot{\boldsymbol{y}} (\dot{\boldsymbol{z}} \cdot \boldsymbol{a})\right] \\ &- C_1 C_2^2 C_3 \left[\dot{\boldsymbol{y}} \cdot (\boldsymbol{a} \times \boldsymbol{b}) \left(\boldsymbol{a} + \boldsymbol{b}\frac{a}{b}\right) \cdot (\dot{\boldsymbol{z}} \times \dot{\boldsymbol{x}}) \right. \\ &+ \left. \dot{\boldsymbol{z}} \cdot (\boldsymbol{a} \times \boldsymbol{b}) \left(\boldsymbol{b} + \boldsymbol{a}\frac{b}{a}\right) \cdot (\dot{\boldsymbol{y}} \times \dot{\boldsymbol{x}})\right] \\ &+ C_1 C_2 \left[\dot{\boldsymbol{y}} \cdot (\boldsymbol{a} \times \boldsymbol{b}) \left(\boldsymbol{b}\frac{c-a}{b^2} + \boldsymbol{c}\frac{a+b}{c^2}\right) \cdot (\dot{\boldsymbol{z}} \times \dot{\boldsymbol{x}}) \right. \\ &+ \left. \dot{\boldsymbol{z}} \cdot (\boldsymbol{a} \times \boldsymbol{b}) \left(\boldsymbol{a}\frac{c-b}{a^2} - \boldsymbol{c}\frac{a+b}{c^2}\right) \cdot (\dot{\boldsymbol{y}} \times \dot{\boldsymbol{x}})\right] \end{aligned} \tag{2.4}$$

$$F_2(\boldsymbol{x}, \boldsymbol{y}, \boldsymbol{z}, \boldsymbol{w}; \dot{\boldsymbol{x}}, \dot{\boldsymbol{y}}, \dot{\boldsymbol{z}}, \dot{\boldsymbol{w}}) = \frac{1}{8\pi^2} \left(\dot{\boldsymbol{x}} \cdot \left(\dot{\boldsymbol{z}} \times \frac{\boldsymbol{b}}{b^3}\right)\right) \left(\dot{\boldsymbol{y}} \cdot \left(\dot{\boldsymbol{w}} \times \frac{\boldsymbol{c}}{c^3}\right)\right) \tag{2.5}$$

In Eqs. (2.4) and (2.5) we have put:

$$\boldsymbol{a} = \boldsymbol{y} - \boldsymbol{x} \qquad \boldsymbol{b} = \boldsymbol{z} - \boldsymbol{x} \qquad \boldsymbol{c} = \boldsymbol{y} - \boldsymbol{z} \tag{2.6}$$

and

$$C_1 = \frac{2\pi}{abc} \tag{2.7}$$

$$C_2 = \frac{1}{ab + a_\mu b_\mu} \tag{2.8}$$

$$C_3 = a + b - c \tag{2.9}$$

Let us note that in Eq. (2.8) we have used a convention for which repeated indices are summed. It is known that $\varrho(C)$ is related to the second coefficient $a_2(C)$ of the Conway polynomial of a knot C through the following relation [16]:

$$a_2(C) = \frac{1}{2}\left[\varrho(C) + \frac{1}{12}\right] \tag{2.10}$$

The coefficients of the Conway polynomials are known for every knot topology. $\varrho(C)$ is also called the Casson knot invariant, see Ref. [37].

3. A Monte Carlo algorithm for computing numerical invariants

In physical applications, where a sum over all the conformations of a knot with fixed topology should be performed in order to compute the partition function, it is possible to use a path integral approach, see for instance [38,39]. Yet, the path integration over all loops $\boldsymbol{x}(s)$ is highly non trivial. For this reason, whenever there are systems in which topological relations play a relevant role, the problem of predicting their properties is mostly tackled with numerical simulations. To that purpose it is necessary to introduce a suitable discrete representation of knots. In the rest of this Section, such representation will be provided together with a general formula for computing multiple line integrals within the Monte Carlo integration scheme. Later, this formula will be applied to the case of the Vassiliev knot invariant of degree 2 of Eq. (2.1).

A discrete knot will be considered here as a set of N points:

$$\boldsymbol{x}_i = \boldsymbol{x}(s_i) \qquad \begin{cases} i = 1, \dots, N \\ 0 < s_1 < s_2 \cdots < s_N = L \end{cases} \tag{3.1}$$

joined together by N segments

$$\boldsymbol{l}_i = \boldsymbol{x}_i - \boldsymbol{x}_{i-1} \qquad i = 2, \dots, N \tag{3.2}$$

$$\boldsymbol{l}_1 = \boldsymbol{x}_1 - \boldsymbol{x}_N \tag{3.3}$$

The discrete knot may be regarded as a piecewise smooth curve $\boldsymbol{X}(S) : [0, N] \longrightarrow \mathbb{R}$, where

$$0 \leq S \leq N \tag{3.4}$$

Explicitly, a general point located on the $i-$th segment of $\boldsymbol{X}(S)$ is identified by the relations:

$$\boldsymbol{X}(S) = \boldsymbol{x}_{i-1} + (S - [S])\boldsymbol{l}_i \qquad \begin{cases} i - 1 < S \leq i \\ i = 2, \dots, N \end{cases} \tag{3.5}$$

and

$$\boldsymbol{X}(S) = \boldsymbol{x}_N + (S - [S])\boldsymbol{l}_1 \qquad 0 < S \leq 1 \tag{3.6}$$

In the above equations $[S]$ denotes the integer part of S. The example of a curve $\boldsymbol{X}(S)$ with eight segments is given in Fig. 2. In the limit in which N approaches infinity and the lengths of the N segments become vanishingly small, a continuous representation of the knot is obtained. If $l_i = |\boldsymbol{l}_i|$ denotes the length of the $i-$th segment and $\Lambda_N = \sum_{i=1}^{N} l_i$ is the total length of the discretized curve, then the length L of the continuous knot is given by:

$$\lim_{\substack{N \to \infty \\ l_i \to 0,\, i=1,\dots,N}} \Lambda_N = L \tag{3.7}$$

At this point it is possible to compute the contributions $\varrho_1(C)$ and $\varrho_2(C)$ to the Vassiliev invariant of degree 2 for a general discrete knot C with path $\boldsymbol{X}(S)$. With

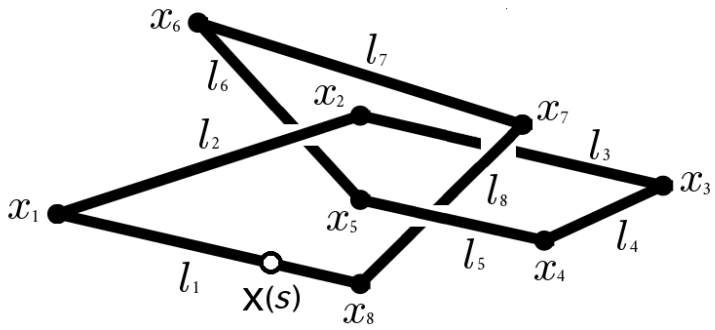

Fig. 2. Example of an off lattice discrete knot (a trefoil) with only eight sides. A generic point $\boldsymbol{X}(S)$ on the loop is shown.

the above definitions, the same prescriptions of Eqs. (2.2) and (2.3), which are valid for a smooth curve $\boldsymbol{x}(s)$, can be formally applied in the present context. It is sufficient to substitute the smooth curves $\boldsymbol{x}(s), \boldsymbol{y}(t), \boldsymbol{z}(u)$ and $\boldsymbol{w}(v)$ with their discrete analogs $\boldsymbol{X}(S), \boldsymbol{Y}(T), \boldsymbol{Z}(U)$ and $\boldsymbol{W}(V)$. In the following, the symbols $F_1(S,T,U)$ and $F_2(S,T,U,V)$ will denote the integrands of Eqs. (2.2) and (2.3) in the case of a discrete knot in which the variables s,t,u,v are replaced by S,T,U,V. Of course, in these equations the upper integration boundary L should be replaced by N. The derivatives $\dot{\boldsymbol{X}}(S), \dot{\boldsymbol{Y}}(T), \dot{\boldsymbol{Z}}(U)$ and $\dot{\boldsymbol{W}}(V)$ require some more care. On the $i-$th segment, away from the joints, the curve is trivially smooth and the computation of $\dot{\boldsymbol{X}}(S), \dot{\boldsymbol{Y}}(T), \dot{\boldsymbol{Z}}(U), \dot{\boldsymbol{W}}(V)$ is straightforward:

$$\dot{\boldsymbol{X}}(S) = \boldsymbol{l}_i \qquad \begin{cases} i-1 < S < i \\ i = 2, \ldots, N \end{cases} \tag{3.8}$$

$$\dot{\boldsymbol{X}}(S) = \boldsymbol{l}_1 \qquad 0 < S < 1 \tag{3.9}$$

At the points $\boldsymbol{x}_1, \ldots, \boldsymbol{x}_N$ in which the segments join together, instead, the curve $\boldsymbol{X}(S)$ ceases to be differentiable. Still, it is possible to define formally the derivatives at these points by assuming that the tangent to the discrete curve in $\boldsymbol{x}_{i-1}$ is proportional to the segment $\boldsymbol{l}_i$. Using this convention we obtain:

$$\dot{\boldsymbol{X}}(i-1) = \boldsymbol{l}_i \qquad\qquad i = 2, \ldots, N \tag{3.10}$$

$$\dot{\boldsymbol{X}}(N) = \boldsymbol{l}_1 \tag{3.11}$$

The above definition is clearly not unique. In an equivalent manner we could have chosen $\dot{\boldsymbol{X}}(i-1) = \boldsymbol{l}_{i-1}$, $i = 2, \ldots, N$ and $\dot{\boldsymbol{X}}(N) = \boldsymbol{l}_N$.

With the prescriptions (3.4–3.6) and (3.8–3.11) given above in order to parametrize the discrete knot, the evaluation of the multiple line integrals appear-

ing in numerical discrete knots, like $\varrho_1(C)$ in Eq. (2.2) and $\varrho_2(C)$ in Eq. (2.3), may be performed using numerical integration techniques. Possible choices are the rectangle rule method, trapezoidal rule method, Simpson's rule method, Newton-Cotes method, Romberg method, Gauss method etc. [40]. The problem of computing the necessary integrals in this way is that the volume spanned by the variables over which we have to sum is huge. Considering again $\varrho(C)$ as a concrete example, this volume is given by

$$V_1 = \frac{N^3}{6} \tag{3.12}$$

in the case of the first integral $\varrho_1(C)$ of Eq. (2.2), while the variables S, T, U and V appearing in $\varrho_2(C)$, see Eq. (2.3), span a space of volume

$$V_2 = \frac{N^4}{24} \tag{3.13}$$

Eq. (3.12) has been obtained by putting in Eq. (2.2) $F_1(\boldsymbol{x}(s), \boldsymbol{y}(t), \boldsymbol{z}(u); \dot{\boldsymbol{x}}(s), \dot{\boldsymbol{y}}(t), \dot{\boldsymbol{z}}(u)) = 1$. In this way the right hand side of Eq. (2.2) becomes an integral over the volume form $dV_1 = dsdtdu$. After computing that integral, the result is $V_1 = \frac{L^3}{6}$. After passing to the dicrete version of the knot and supposing that all the N segments composing the discrete knot have the same length l, we obtain $V_1 = \frac{(Nl)^3}{6}$. Eq. (3.12) corresponds to the particular case in which all segments have unit length, i. e. $l = 1$. Eq. (3.13) has been derived in an analogous way. V_1 and V_2 provide good measures of how the number of points to be considered when $\varrho_1(C)$ and $\varrho_2(C)$ are computed with the standard integration methods grows with growing values of N.

When N is large, the volumes V_1 and V_2 become too large to be treated with quadrature methods and it is more convenient to compute the right hand sides of Eqs. (2.2) and (2.3) using a Monte Carlo approach[b]. Let us consider at this point multiple contour integrals in which the contour is the curve describing a knot conformation. The curve may be parametrised by any parameter ξ. ξ could be for instance the arc-length, i. .e. $\xi = s$, or in the case of a discrete knot $\xi = S$. After choosing a suitable parametrisation, the multiple countour integral becomes that of a function of m variables $f(\xi_1, \cdots, \xi_m)$ with integration boundaries like those in Eqs. (2.2) and (2.3). To evaluate the integral it is possible to apply the Monte Carlo formula:

$$\begin{aligned} &\int_{a_1}^{b_1} d\xi_1 \int_{a_2}^{\xi_1} d\xi_2 \cdots \int_{a_m}^{\xi_{m-1}} d\xi_m f(\xi_1, \cdots, \xi_m) \\ &\approx \frac{1}{n} \left[\sum_{\nu=1}^{n} f(\xi_1^{(\nu)}, \cdots, \xi_m^{(\nu)})(b_1 - a_1) \prod_{s=2}^{m} (\xi_{s-1}^{(\nu)} - a_s) \right] \end{aligned} \tag{3.14}$$

[b]Nonstandard methods like that based on Particle Swarm Optimization proposed in [40] could probably also be successfully applied.

where the index $\nu = 1, \cdots, n$ numbers the $\nu-$th sample of the parameters $\xi_1, \ldots, \xi_m$ and $s = 1, \cdots, m$. The $\xi_s^{(\nu)}$'s are randomly sampled with an uniform distribution in the following intervals:

$$\begin{array}{l} \xi_1^{(\nu)} \in [a_1, b_1] \\ \xi_s^{(\nu)} \in [a_s, \xi_{s-1}] \text{ when } s = 2, \ldots, m \end{array} \tag{3.15}$$

The details of the sampling procedure will be provided later in Section 7. Here we consider numerical knot invariants Ξ that may be reduced in the general form of a linear combination of K multiple integrals:

$$\Xi = \sum_{z=1}^{K} \int_{a_1^{(z)}}^{b_1^{(z)}} d\xi_1 \int_{a_2^{(z)}}^{\xi_1} d\xi_2 \cdots \int_{a_m^{(z)}}^{\xi_{(m^{(z)}-1)}} d\xi_{m^{(z)}} f^{(z)}(\xi_1, \ldots, \xi_{m^{(z)}}) \tag{3.16}$$

Let us notice that in the above formula we have taken into account the general situation in which the boundary limits of the integrations depend on the index $z = 1, \ldots, K$. The approximate value $\langle \Xi \rangle$ of Ξ is obtained after computing each of the multiple integrals in the right hand side of Eq. (3.16) by applying the Monte Carlo formula of Eq. (3.14). To evaluate each of the K integrals appearing in Eq. (3.16) we choose the same number of sampling points n. In a similar way it is possible to evaluate the variance:

$$\sigma^2 = \langle \Xi^2 \rangle - \langle \Xi \rangle^2 \tag{3.17}$$

The standard deviation σ is important in order to estimate how close is the result $\langle \Xi \rangle$ from the exact value of Ξ for a given knot C.

The naive procedure discussed above is plagued by two systematic errors. First of all, the discrete knots treated here are not smooth at the joints between two segments. This spoils the calculation of numerical topological invariants. For instance, we have verified on a simple cubic lattice that the values of $\varrho(C)$ computed for a discrete knot are always greater than the exact values, a fact that is certainly related to the presence of sharp corners at these joints. This excess from the exact value is indeed roughly proportional to the number of corners.

The second source of errors is connected with possible singularities arising in some of the terms appearing in the integrands $f^{(z)}(\xi_1, \ldots, \xi_{m^{(z)}})$, $z = 1, \ldots, K$, of Eq. (3.16). Of course, these singularities cancel out when considering the whole sum of integrands because the value of a knot invariant should be finite. However, the fact that single terms could become arbitrarily large is not easy to handle in numerical calculations and may endanger the obtained results. To avoid this to happen, a regularization is needed to remove all potential singularities. A convenient regularization is the framing of paths described in [35]. To illustrate how the discretised version of framing works, we consider $\varrho(C)$ as an example. In this case both integrands $F_1(S, T, U)$ and $F_2(S, T, U, V)$ of Eqs. (2.2) and (2.3) respectively are regular for every value of S, T, U and V as it has been proved in [16]. Yet, some of the terms entering the expressions of $F_1(S, T, U)$ and $F_2(S, T, U, V)$ could

become divergent. Looking at Eqs. (2.4–2.9), it is easy to realize that divergences may indeed occur whenever one or more of the following conditions are met:

$$\boldsymbol{Y}(T) - \boldsymbol{X}(S) = 0 \tag{3.18}$$

$$\boldsymbol{Z}(U) - \boldsymbol{X}(S) = 0 \tag{3.19}$$

$$\boldsymbol{Y}(T) - \boldsymbol{Z}(U) = 0 \tag{3.20}$$

$$|\boldsymbol{Y}(T) - \boldsymbol{X}(S)|\,|\boldsymbol{Z}(U) - \boldsymbol{X}(S)| + (\boldsymbol{Y}(T) - \boldsymbol{X}(S)) \cdot (\boldsymbol{Z}(U) - \boldsymbol{X}(S)) = 0 \tag{3.21}$$

The framing consists in a slight deformation of the curves $\boldsymbol{X}(S)$, $\boldsymbol{Y}(T)$, $\boldsymbol{Z}(U)$ and $\boldsymbol{W}(V)$:

$$X^{\mu}(S) \longrightarrow X^{\mu}_{\epsilon_X}(S) = X^{\mu}(S) + \epsilon n^{\mu}(S) \tag{3.22}$$

$$Y^{\nu}(T) \longrightarrow Y^{\nu}_{\epsilon_Y}(T) = Y^{\nu}(T) + 2\epsilon n^{\nu}(T) \tag{3.23}$$

$$Z^{\rho}(U) \longrightarrow Z^{\rho}_{\epsilon_Z}(U) = Z^{\rho}(U) + 3\epsilon n^{\rho}(U) \tag{3.24}$$

$$W^{\sigma}(V) \longrightarrow W^{\sigma}_{\epsilon_W}(V) = W^{\sigma}(V) + 4\epsilon n^{\sigma}(V) \tag{3.25}$$

where $n^{\mu}(S), n^{\nu}(T), n^{\rho}(U)$ and $n^{\sigma}(V)$ denote unit vectors normal to the curves $\boldsymbol{X}(S)$, $\boldsymbol{Y}(T)$, $\boldsymbol{Z}(U)$ and $\boldsymbol{W}(V)$ respectively. ϵ is a very small parameter. Clearly, the prescription provided in Eqs. (3.22–3.25) is able to remove the divergences at the locations defined in (3.18–3.21). Moreover, in the limit $\epsilon \to 0$, one recovers the exact expression of $\varrho(C)$ independently of the choice of the normal unit vectors $n^{\mu}(S), n^{\nu}(T), n^{\rho}(U)$ and $n^{\sigma}(V)$ as it has been proved in Ref. [16]. For example, in calculations on a simple cubic lattice the framing can be implemented by small shifts of the paths $\boldsymbol{X}(S)$, $\boldsymbol{Y}(T)$, $\boldsymbol{Z}(U)$ and $\boldsymbol{W}(V)$ along the direction $(1, 1, 1)$. If ϵ is sufficiently small, it is possible to regularize all potentially divergent terms in $F_1(S, T, U)$ and $F_2(S, T, U, V)$ without introducing undesired intersections between the lines of the shifted knots. Obviously, these intersections should be forbidden. From our simulations it turns out that the results of the computations of $\varrho(C)$ are not much sensitive to the values of the $\epsilon-$parameter. This is connected to the fact that the points in which the singularity conditions of Eqs. (3.18–3.21) are satisfied represent a very small subset of the set of all sampled points. Yet, untreated singularities at these points could generate large terms and eventually affect the entire evaluation of $\varrho(C)$.

To eliminate the systematic error due to the presence of the sharp corners is much more difficult. This will be the subject of the next Section, in which a smoothing procedure will be presented that transforms C^0 curves into G^1-curves.

4. A fast smoothing procedure for dicrete knots

In the previous Section the fundamental formulas for the evaluation of numerical topological invariants in the case of discrete loops $\boldsymbol{X}(S)$ have been provided. The discretization process is needed in order to apply invariants of this type to numerical simulations, where knots are typically represented as systems of segments joined together. Yet, while it is perfectly fine to have knots with sharp corners,

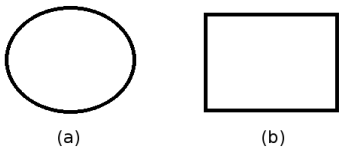

Fig. 3. (a) An unknot with smooth path; (b) An unknot defined on a simple cubic lattice.

this representation is not entirely suitable to the main purpose for which numerical knot invariants are used. Indeed, if the topology of a knot has to be determined with the help of numerical knot invariants, then the fact that the knot is not described by a smooth curve becomes an obstacle. The problem is that such knot invariants are expressed in the form of multiple line integrals like $\varrho(C)$ and cease to be topological invariants if knots are smooth only piecewise. In the next Section it will be shown more in details taking $\varrho(C)$ as an example how the computation of numerical topological invariants in this case does not provide reliable results. As a consequence, a procedure that is able to smooth up a discrete knot so that numerical topological invariants could be used is highly necessary. This is the subject of this Section. We will prove here that to this aim it is sufficient to transform the C^0-curve representing a discrete knot $\boldsymbol{X}(S)$ into a G^1-curve.

The effect of the sharp corners at the joints of the segments on the computation of $\varrho(C)$ can be checked using the very simple example of an unknot with two different conformations:

- A smooth circle defined by the parametric curve $x^1(\theta) = \cos(\theta)$, $x^2(\theta) = \sin(\theta)$ and $x^3(\theta) = 0$, $\theta \in [0, 2\pi]$, see Fig. 3(a).
- A square defined on a simple cubic lattice as shown in Fig. 3(b).

The exact value of the Vassiliev invariant of degree 2 for the unknot is $-\frac{1}{12} \sim -0.083$. The Monte Carlo computation of $\varrho(C)$ gives a result that is very near to the exact one in the case of the circle: $\varrho(C) = -0.083 \pm 1.72 \times 10^{-4}$. However, for the square we obtain $\varrho(C) = 0.050 \pm 1.17 \times 10^{-4}$, which is far from the expected result. To avoid these ambiguities in the calculation of numerical topological invariants for discrete knots like $\varrho(C)$, a smoothing procedure for eliminating the sharp corners will be presented.

The idea is to replace the sharp corners at the joints $\boldsymbol{x}_i$ with arcs of smooth curves. To illustrate the method, we pick up a triplet of contiguous segments $\boldsymbol{l}_{i-1}, \boldsymbol{l}_i$ and $\boldsymbol{l}_{i+1}$, see Fig. 4. The two corners to be smoothed up appearing in the figure are respectively formed by the contiguous segments $\boldsymbol{l}_{i-1}, \boldsymbol{l}_i$ and $\boldsymbol{l}_i, \boldsymbol{l}_{i+1}$. At this point

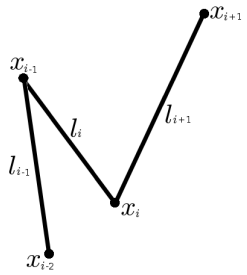

Fig. 4. This figure shows the three contiguous segments $\boldsymbol{l}_{i-1}, \boldsymbol{l}_i$ and $\boldsymbol{l}_{i+1}$ subtending the corners $\boldsymbol{x}_{i-1}$ and $\boldsymbol{x}_i$.

we further divide each segment $\boldsymbol{l}_i$, $i = 1, \ldots, N$, into three subsegments:

$$\boldsymbol{l}_i^- = \boldsymbol{x}_i^- - \boldsymbol{x}_{i-1} \tag{4.1}$$

$$\boldsymbol{l}_i^0 = \boldsymbol{x}_i^+ - \boldsymbol{x}_i^- \tag{4.2}$$

$$\boldsymbol{l}_i^+ = \boldsymbol{x}_i^+ - \boldsymbol{x}_i \tag{4.3}$$

Considering Fig. 5 in order to fix the ideas, the corners subtended by the subsegments $\boldsymbol{l}_{i-1}^+, \boldsymbol{l}_i^-$ and $\boldsymbol{l}_i^+, \boldsymbol{l}_{i+1}^-$ will be substituted with arcs of smooth functions as shown in Fig. 6. This procedure will be repeated for each corner subtended by the couples of segments $\boldsymbol{l}_i^+, \boldsymbol{l}_{i+1}^-$ for $i = 1, \ldots, N-1$ and $\boldsymbol{l}_N^+, \boldsymbol{l}_1^-$ for $i = N$.

The ends $\boldsymbol{x}_i^-$ and $\boldsymbol{x}_i^+$ are fixed in such a way that the lengths of $\boldsymbol{l}_i^-, \boldsymbol{l}_i^0$ and $\boldsymbol{l}_i^+$ are d'_{i-1}, $l_i - d'_{i-1} - d_i$ and d_i respectively:

$$\boldsymbol{x}_i^- = \boldsymbol{x}_{i-1} + \frac{\boldsymbol{x}_i - \boldsymbol{x}_{i-1}}{l_i} d'_{i-1} \tag{4.4}$$

$$\boldsymbol{x}_i^+ = \boldsymbol{x}_i + \frac{\boldsymbol{x}_{i-1} - \boldsymbol{x}_i}{l_i} d_i \tag{4.5}$$

The values of d'_{i-1} and d_i will be chosen in such a way that

1) the topology of the discrete knot is not destroyed after the smoothing procedure and

2) the length of none of the subsegments $\boldsymbol{l}_i^{\pm}$ and $\boldsymbol{l}_i^0$ exceeds $\frac{l_i}{2}$.

An algorithm to determine d'_{i-1} and d_i will be provided later. After performing the above splitting for $\boldsymbol{l}_{i-1}$, $\boldsymbol{l}_i$ and $\boldsymbol{l}_{i+1}$, the subsegments $\boldsymbol{l}_{i-1}^+$ and $\boldsymbol{l}_i^-$ subtend the corner centered in $\boldsymbol{x}_{i-1}$, while the corner in $\boldsymbol{x}_i$ is subtended by $\boldsymbol{l}_i^+$ and $\boldsymbol{l}_{i+1}^-$.

The smooth arcs that will replace the corners at the points $\boldsymbol{x}_i$, $i = 1, \ldots, N$,

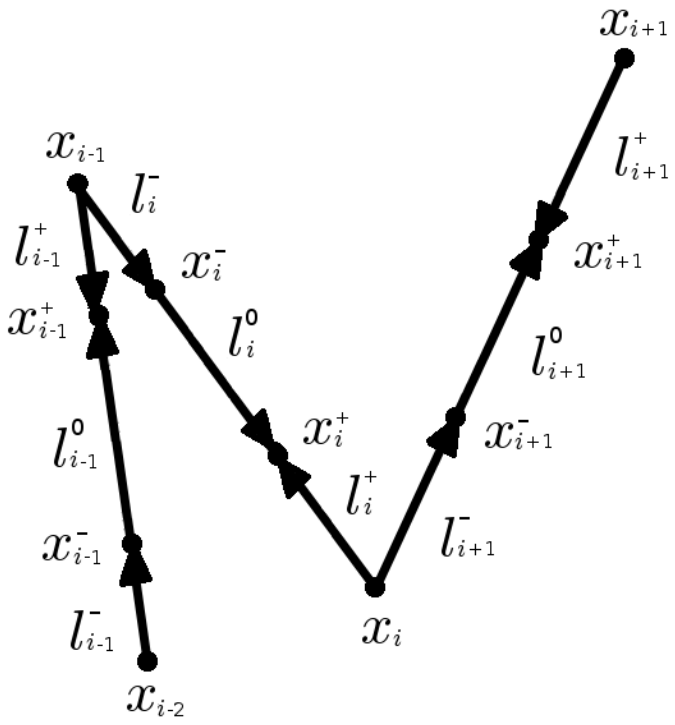

Fig. 5. The segments $\boldsymbol{l}_{i-1}, \boldsymbol{l}_i$ and $\boldsymbol{l}_{i+1}$ of Fig. 4 are split into three subsegments in such a way that the corners in $\boldsymbol{x}_{i-1}$ and $\boldsymbol{x}_i$ are subtended by segments that are not in common. In the given example, after the splitting, the corner in $\boldsymbol{x}_{i-1}$ is subtended by the subsegments $\boldsymbol{l}_{i-1}^+$ and $\boldsymbol{l}_i^-$. The corner in $\boldsymbol{x}_i$ is subtended instead by $\boldsymbol{l}_i^+$ and $\boldsymbol{l}_{i+1}^-$.

subtended by the subsegments $\boldsymbol{l}_i^+$ and $\boldsymbol{l}_{i+1}^-$ are defined in parametric form as follows:

$$\begin{aligned}\boldsymbol{X}_i^+(S) = &-\frac{d_i}{l_i}\frac{l_{i+1}}{d_i'}\frac{\sin\theta_i^+(S)}{1-\frac{1}{\sqrt{2}}+\frac{1}{\sqrt{2}}\frac{d_i}{l_i}\frac{l_{i+1}}{d_i'}}\boldsymbol{l}_i^+ \\ &-\frac{(\cos\theta_i^+(S)-1)}{1-\frac{1}{\sqrt{2}}+\frac{1}{\sqrt{2}}\frac{l_i}{d_i}\frac{d_i'}{l_{i+1}}}\boldsymbol{l}_{i+1}^- + \boldsymbol{l}_i^+ + \boldsymbol{x}_i \qquad (4.6)\\ \boldsymbol{X}_{i+1}^-(S) = &-\frac{(\sin\theta_{i+1}^-(S)-1)}{1-\frac{1}{\sqrt{2}}+\frac{1}{\sqrt{2}}\frac{d_i}{l_i}\frac{l_{i+1}}{d_i'}}\boldsymbol{l}_i^+ \\ &-\frac{l_i}{d_i}\frac{d_i'}{l_{i+1}}\frac{\cos\theta_{i+1}^-(S)}{1-\frac{1}{\sqrt{2}}+\frac{1}{\sqrt{2}}\frac{l_i}{d_i}\frac{d_i'}{l_{i+1}}}\boldsymbol{l}_{i+1}^- + \boldsymbol{l}_{i+1}^- + \boldsymbol{x}_i \qquad (4.7)\end{aligned}$$

with

$$\theta_i^+(S) = \left(\frac{l_i}{2d_i}(S-[S]) - \frac{l_i-d_i}{2d_i}\right)\frac{\pi}{2} \qquad \frac{l_i-d_i}{l_i} \leq S-[S] \leq 1 \quad (4.8)$$

$$\theta_{i+1}^-(S) = \left(\frac{l_{i+1}}{2d_i'}(S-[S]) + \frac{1}{2}\right)\frac{\pi}{2} \qquad 0 \leq S-[S] \leq \frac{d_i'}{l_{i+1}} \quad (4.9)$$

Eqs. (4.6–4.9) are defined for $i = 1, \ldots, N-1$. Their extension to the corner in $\boldsymbol{x}_N$ is straightforward. In these formulas the superscript + refers to the arc of the curve replacing the segment $\boldsymbol{l}_i^+$, while the superscript − refers analogously to $\boldsymbol{l}_{i+1}^-$.

It is easy to verify that, after replacing the sharp corners at the vertices $\boldsymbol{x}_i$ with the arcs $\boldsymbol{X}_i^+(S)$ and $\boldsymbol{X}_{i+1}^-(S)$, a G^1-curve is obtained:

(1) First of all, at the point in which $\boldsymbol{X}_i^+(S)$ and $\boldsymbol{X}_{i+1}^-(S)$ are joined together, identified by the condition $\theta_i^+(1) = \theta_{i+1}^-(0) = \frac{\pi}{4}$, it is possible to verify that the curve obtained after the replacement is continuous.
(2) Second, both $\boldsymbol{X}_i^+(S)$ and $\boldsymbol{X}_{i+1}^-(S)$ are differentiable and their derivatives, which are continuous too, coincide.
(3) Third, at the point $\boldsymbol{x}_i^+$ in which the arc $\boldsymbol{X}_i^+(S)$ and the subsegment l_i^0 are joined together, the unit vector that is tangent to $\boldsymbol{l}_i^0$ coincides with the unit vector that is tangent to $\boldsymbol{X}_i^+(S)$. A similar statement is true in the case of the junction point $\boldsymbol{x}_i^-$ between $\boldsymbol{X}_i^-(S)$ and $\boldsymbol{l}_i^0$. To show that, we note that $\boldsymbol{X}_i^+(S)$ maps the subsegment $\boldsymbol{l}_i^+$ into a continuous arc of a curve with unit tangent vector $\boldsymbol{t}_i^+$ at the end point $\boldsymbol{x}_i^+$ given by $\boldsymbol{t}_i^+ = -\frac{\boldsymbol{l}_i^+}{l_i^+}$. To have a G^1-curve, $\boldsymbol{t}_i^+$ must coincide with the tangent $\boldsymbol{t}_i^0$ computed at $\boldsymbol{x}_i^+$, but staying on the subsegment $\boldsymbol{l}_i^0$. It is easy to check using the parametrization (3.5–3.6) of the knot on $\boldsymbol{l}_i^0$ that $\boldsymbol{t}_i^0 = \frac{\boldsymbol{l}_i}{l_i}$. Thus, taking into account the fact that $\boldsymbol{l}_i^+$ and $\boldsymbol{l}_i$ are antiparallel, it is possible to conclude that $\boldsymbol{t}_i^+ = \boldsymbol{t}_i^0$ as desired. In a similar way it is possible to prove that the unit tangent vector computed on the curve $\boldsymbol{X}_{i+1}^-(S)$ at $\boldsymbol{x}_{i+1}^-$ coincides with the unit tangent vector computed on $\boldsymbol{l}_{i+1}^0$ at the point $\boldsymbol{x}_{i+1}^-$.
(4) Finally, we have also checked numerically that, for a wide range of the variable $x = \frac{d_i l_{i+1}}{d_{i+1} l_i}$ entering the expressions of $\boldsymbol{X}_i^+(S)$ and $\boldsymbol{X}_{i+1}^-(S)$, more precisely for $0.01 \leq x \leq 100$, the distance between the point $\boldsymbol{x}_i$ in which the original corner to be substituted was centered and any of the points of the arc of the curve $\boldsymbol{X}_i^+(S)$ ($\boldsymbol{X}_{i+1}^-(S)$) that has replaced the subsegment $\boldsymbol{l}_i^+$ ($\boldsymbol{l}_i^-$) never grows beyond a fraction of d_i (d_i'). This fact will be used in the next Section to endow the smoothing procedure with a topology preservation algorithm. Moreover, since the path of the smooth arc sticks very close to the path of the old discrete knot, it is more likely that the topology of the knot obtained after smoothing a sharp corner will not be destroyed if the length of this arc is increased to cover the largest possible region. This is very relevant for speeding up the Monte Carlo calculation of numerical topological invariants. In fact, if only very small portions of the knot around the centers of the corners $\boldsymbol{x}_i$, $i = 1, \ldots, N$ may

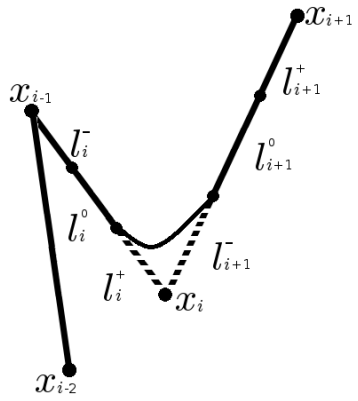

Fig. 6. Substitution of the sharp corner in $\boldsymbol{x}_i$ by an arc of the smooth curve defined in Eqs. (4.6–4.7). It is shown that the subsegments $\boldsymbol{l}^+_i$ and $\boldsymbol{l}^-_{i+1}$ subtending this corner are replaced by a smooth path. The replaced part has been denoted with dashed lines.

be replaced because otherwise the knot topology is modified, at the end the smoothed version of the knot will coincide with the original discrete knot almost everywhere apart from tiny arcs of a smooth curve around the points $\boldsymbol{x}_i$. If this happens, a more extensive sampling is certainly necessary in order to explore these arcs which, on the other side, are fundamental in order to ensure that the Monte Carlo evaluation of a numerical knot invariant delivers the correct result.

Concluding, after the smoothing procedure presented in this Section 4 is completed, the path of the discrete knot becomes a G^1-curve. At least in the case of the Vassiliev knot invariant of degree 2, we will see that this is sufficient in order to remove all the systematic errors related to the presence of the sharp corners.

5. Adding topology preservation to the smoothing algorithm

The greatest challenge when smoothing a knot is to avoid potential changes in its topology. Any smoothing procedure is in fact potentially dangerous in this respect, especially if the segments composing the knot are allowed to get arbitrarily close to each other as it happens in off-lattice simulations. An example of dangerous situation in which the topology of the knot is modified after the replacement of the sharp corners with arcs of a smooth curve is illustrated in Fig. 7. In the previous Section we have verified that the knot obtained after substituting the region around the sharp corners with arcs is a G^1-curve. We have still to ensure that the topology

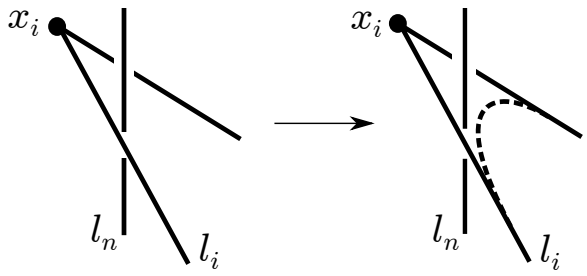

Fig. 7. A situation that should be avoided: before the smoothing of the corner in the point $\boldsymbol{x}_i$, the segment $\boldsymbol{l}_n$ was passing under the segment $\boldsymbol{l}_i$. After smoothing, the segment $\boldsymbol{l}_i$ has been replaced by an arc of a smooth curve in such a way that the segment $\boldsymbol{l}_n$ now passes over that arc, potentially changing the topology of the knot.

of the knot before and after the smoothing procedure remains unaltered. This goal will be achieved here by a careful definition of the lengths d_i and d'_i of the subsegments $\boldsymbol{l}_i^{\pm}$. In practice, the subsegments $\boldsymbol{l}_i^{\pm}$ to be replaced have to be chosen to be short enough, that their arc replacements $\boldsymbol{X}_i^{\pm}(S)$ will not modify the knot type avoiding situations like that in Fig. 7. From the remarks made in point 4 at the end of the previous Section, see page 15, we already know that for calculation purposes it is desirable that d_i and d'_i are as large as possible. We have also seen that the ansatz (4.6-4.7) is very convenient for that purpose, because the loop obtained after smoothing sticks close to the path of the original knot.

In the following, an algorithm to derive suitable values d_i, d'_i for $i = 1, \ldots, N$ will be provided. Strictly speaking, the presented procedure is valid only for $i = 1, \ldots, N-1$. but this is for a pure technical reason. The problem when dealing with the case $i = N$ is that the segment $\boldsymbol{l}_N$ is followed by $\boldsymbol{l}_1$ and not by $\boldsymbol{l}_{N+1}$. The solution is simply to add an extra segment $\boldsymbol{l}_{N+1}$ and to identify it with $\boldsymbol{l}_1$. This is a trivial modification of the procedure.

The lengths d_i, d'_i are determined starting from the first corner located in $\boldsymbol{x}_1$ and then proceeding recursively with the next corners $\boldsymbol{x}_2, \boldsymbol{x}_3, \ldots$ At each joint $\boldsymbol{x}_i$, we should check first of all if $\boldsymbol{l}_i$ and $\boldsymbol{l}_{i+1}$ are parallel or not. If they are parallel, i. e. $\frac{\boldsymbol{l}_i \cdot \boldsymbol{l}_{i+1}}{l_i l_{i+1}} = 1$, this simply means that $\boldsymbol{l}_i$ and $\boldsymbol{l}_{i+1}$ are just forming a longer segment and there is no sharp corner. As a consequence, no action is required and it is possible to pass to the next corner in $\boldsymbol{x}_{i+1}$. Thus, we concentrate to the case in which the two contiguous segments at the $i-$th joint are not parallel.

Starting from $i = 1$, the first task is to find the point $\boldsymbol{x}_{k,1}$ belonging to the knot which is nearest to the joint $\boldsymbol{x}_1$. Let's denote with $d_{k,1}$ the distance between $\boldsymbol{x}_{k,1}$ and $\boldsymbol{x}_1$. The composite index $k, 1$ is used to remember that the point $\boldsymbol{x}_{k,1}$ is lying on the segment $\boldsymbol{l}_k$ with $k \neq 1, 2$ and that it is the nearest point to $\boldsymbol{x}_1$. The restriction $k \neq 1, 2$ is needed to exclude trivial nearest points belonging to the segments $\boldsymbol{l}_1$ and $\boldsymbol{l}_2$.

The technical details of how the position of $\boldsymbol{x}_{k,1}$ and its distance $d_{k,1}$ from $\boldsymbol{x}_1$

are computed are presented in the Appendix. After $\boldsymbol{x}_{k,1}$ and $d_{k,1}$ are known, we choose the lengths d_1 and d_1' of the subsegments $\boldsymbol{l}_1^+$ and $\boldsymbol{l}_2^-$ that will be replaced by arcs of smooth curves as follows:

$$d_1 = d_1' = \min\left\{d_{k,1}, \min\left\{\frac{l_1}{2}, \frac{l_2}{2}\right\}\right\} \tag{5.1}$$

In words, d_1 is set to be equal to d_1'. Moreover, depending on the distance $d_{k,1}$ of the point $\boldsymbol{x}_{k,1}$ from $\boldsymbol{x}_1$ and on the lengths of the segments $\boldsymbol{l}_1, \boldsymbol{l}_2$, we can have the three different possibilities displayed in Fig. 8. Fig. 8 (b) refers to the case in which $l_1 < l_2$ and $d_{k,1} \geq \frac{l_1}{2}$. Fig. 8 (c) shows the analogous situation in which $l_2 \leq l_1$ and $d_{k,1} \geq \frac{l_2}{2}$. In both cases, according to the prescription (5.1), the lengths d_1, d_1' can never be greater than half of the length of the shortest segment between $\boldsymbol{l}_1$ and $\boldsymbol{l}_2$. When $d_{k,1} \leq \min\left\{\frac{l_1}{2}, \frac{l_2}{2}\right\}$, we have the situation depicted in Fig. 8 (a). Eq. (5.1) implies that $d_{k,1}$ cannot be greater than $\min\left\{\frac{l_1}{2}, \frac{l_2}{2}\right\}$. This requirement is not strictly necessary. It has been added just to limit the lengths of the subsegments $\boldsymbol{l}_i^+, \boldsymbol{l}_{i+1}^-$ to be less or equal to half of the total length of the shortest between the two segments $\boldsymbol{l}_i, \boldsymbol{l}_{i+1}$. Let us notice that, if the values d_1, d_1' are selected according to Eq. (5.1), then both subsegments $\boldsymbol{l}_1^+$ and $\boldsymbol{l}_2^-$, lie inside a sphere $S_{\boldsymbol{x}_1}$ of radius d_1 centered in $\boldsymbol{x}_1$. Moreover, this sphere contains also the arc of a smooth curve replacing the segments $\boldsymbol{l}_1^+$ and $\boldsymbol{l}_2^-$ (see point 4 of the previous Section on page 15). Finally, in the worse situation in which $d_1 = d_{k,1}$, the point $\boldsymbol{x}_{k,1}$ will be located at the border of the sphere. This is very important in order to prevent breakings of topology. In fact, since $\boldsymbol{x}_{k,1}$ is the point on the knot which is nearest to $\boldsymbol{x}_1$ excluding the points on the replaced segments $\boldsymbol{l}_1^+$ and $\boldsymbol{l}_2^-$, this implies that no unwanted segment or part of it can be inside $S_{\boldsymbol{x}_1}$. In summary, dangerous situations such as those presented in Fig. 7 are not possible.

Now we suppose that all the values of $d_j = d_j'$ have been computed up to $j < i$. Implicitly, excluding corners in which the segments $\boldsymbol{l}_{j-1}, \boldsymbol{l}_j$ are parallel, we should assume that the subsegments $\boldsymbol{l}_j^\pm$ with $j < i$ and $\boldsymbol{l}_i^-$ have already been replaced by the smooth arcs of Eqs. (4.6–4.7). We also assume that the smoothing procedure has been carried out in such a way that, for $j < i-1$, the arcs substituting the subsegments $\boldsymbol{l}_j^+, \boldsymbol{l}_{j+1}^-$ are inside a sphere $S_{\boldsymbol{x}_j}$ of radius d_j and no other part of the knot after the replacements made so far can be inside this sphere. The same statement is valid in the case $j = i-1$ too, so that the sphere S_{i-1} of radius d_{i-1} contains only the arcs of curves which replaced the subsegments $\boldsymbol{l}_{i-1}^+, \boldsymbol{l}_i^-$.

At this point we have to deal with the corner corresponding to the vertex in $\boldsymbol{x}_i$. As we did for the first corner in $\boldsymbol{x}_1$, we determine the position of the point which is nearest to $\boldsymbol{x}_i$ and does not belong to $\boldsymbol{l}_i$ or $\boldsymbol{l}_{i+1}$. First, we deal with the case in which this point is on a part of the knot that is unaffected by the smoothing procedure. Let us call this point $\boldsymbol{x}_{l,i}$. Its distance from the center of the corner to be replaced $\boldsymbol{x}_i$ will be denoted with the symbol $d_{l,i}$. $\boldsymbol{x}_{l,i}$ may be located on one of the segments of the knot that have still to be smoothed, i. e. $l > i$, or in the subsegments $\boldsymbol{l}_k^0$ with $k < i$ that have been left unaffected by the smoothing process. The last possibility is

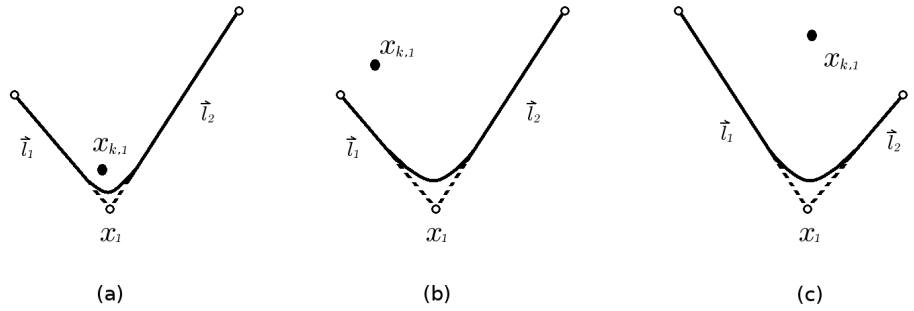

Fig. 8. This set of pictures illustrates the meaning of Eq. (5.1). In panel (a) the point $\boldsymbol{x}_{k,1}$ of the knot, which is nearest point to the vertex $\boldsymbol{x}_1$, is located at a distance $d_{k,1}$ from $\boldsymbol{x}_1$ that is less than $\min\left\{\frac{l_1}{2}, \frac{l_2}{2}\right\}$. In this case the length of the segments $\boldsymbol{l}_1^+$ and $\boldsymbol{l}_2^-$ to be replaced by arcs of smooth curves in order to eliminate the sharp corner in $\boldsymbol{x}_1$ (represented with dashed lines) is chosen to be equal to $d_{k,1}$. The arc of smooth curve with parametric equations (4.6–4.7) replacing $\boldsymbol{l}_1^+$ and $\boldsymbol{l}_2^-$ is constructed in such a way that all of its points are at distances that cannot exceed $d_{k,1}$. As a consequence, this arc is entirely inside the sphere $S_{\boldsymbol{x}_1}$ of radius $d_1 = d_1' = d_{k,1}$. Panels (b-c) describe two situations in which $\boldsymbol{x}_{k,1}$ is at a distance $d_{k,1}$ from $\boldsymbol{x}_1$ which is greater than $\min\left\{\frac{l_1}{2}, \frac{l_2}{2}\right\}$. In this case the length of the segments $\boldsymbol{l}_1^+$ and $\boldsymbol{l}_2^-$ is chosen to be equal to half of the length of the shortest among the segments $\boldsymbol{l}_1$ and $\boldsymbol{l}_2$. Next $\boldsymbol{l}_1^+$ and $\boldsymbol{l}_2^-$ are replaced with arcs of smooth curves. Now the replaced arc lies by construction inside a sphere $S_{\boldsymbol{x}_1}$ whose radius is given by: $d_1 = d_1' = \min\left\{\frac{l_1}{2}, \frac{l_2}{2}\right\}$

that $\boldsymbol{x}_{l,i}$ lies on two contiguous segments $\boldsymbol{l}_j, \boldsymbol{l}_{j+1}$ with $j+1 < i$ that are parallel, so they have been left untreated. The second case is that in which the nearest point to $\boldsymbol{x}_i$ lies on the smooth arc that has replaced the portion of the knot centered at some sharp corner $\boldsymbol{x}_l$, with $l < i$. Let us call this point $\boldsymbol{x}'_{l,i}$ with a prime to remember that it is on a smooth arc and not on the original discrete knot. Despite the fact that the shape of this arc is much more complicated than that of two freely jointed segments, we know that this portion of the new knot obtained after smoothing is confined within the sphere $S_{\boldsymbol{x}_l}$ of radius d_l and $l < i$. For this reason, instead of computing the distance between $\boldsymbol{x}'_{l,i}$ and $\boldsymbol{x}_i$, for practical purposes it is much more convenient to compute the minimal distance between $\boldsymbol{x}_i$ and the sphere $S_{\boldsymbol{x}_l}$. This distance is given by $d_{\boldsymbol{x}_l\boldsymbol{x}_i} - d_l$, where $d_{\boldsymbol{x}_l\boldsymbol{x}_i}$ denotes the distance between the points $\boldsymbol{x}_l$ and $\boldsymbol{x}_i$ and d_l is the radius of the sphere $S_{\boldsymbol{x}_l}$ centered around the point $\boldsymbol{x}_l$. To distinguish the situations in which the nearest point to $\boldsymbol{x}_i$ is a point $\boldsymbol{x}_{l,i}$ in the unchanged part of the knot or a point $\boldsymbol{x}'_{l,i}$ in the part that has been affected by smoothing, we define the following new distance d_i^*:

$$d_i^* = \min_{k=1,\ldots,i-1} \{d_{l,i}, d_{\boldsymbol{x}_k\boldsymbol{x}_i} - d_k\} \tag{5.2}$$

The meaning of d_i^* is illustrated in Figs. 9 and 10.

The radius d_i of the sphere $S_{\boldsymbol{x}_i}$ surrounding the sharp corner in $\boldsymbol{x}_i$ to be replaced

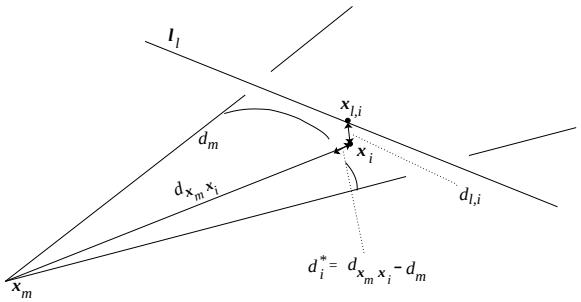

Fig. 9. This picture explains the meaning of the quantity d_i^* appearing in Eq. (5.2). We suppose here that $m < i$ is the value of the index $k = 1, \ldots, i-1$ that minimizes the difference $d_{\boldsymbol{x}_k \boldsymbol{x}_i} - d_k$ and that this difference is smaller than $d_{l,i}$, see Eq. (5.2). This means that after the points $\boldsymbol{x}_k$ with $k < i$ have undergone the smoothing process, the surface of the sphere $S_{\boldsymbol{x}_m}$ centered around $\boldsymbol{x}_m$ has a point that it is nearer to $\boldsymbol{x}_i$, the center of the corner to be smoothed, than the point $\boldsymbol{x}_{l,i}$. The latter is the point lying on the path of the knot that is nearest to $\boldsymbol{x}_i$. The distance between $\boldsymbol{x}_{l,i}$ and $\boldsymbol{x}_i$ is $d_{l,i}$. In order to perform a safe smoothing of the corner around $\boldsymbol{x}_i$ we need to surround it with a sphere of a suitable radius d_i such that does not contain any point of the knot. This is to avoid unwanted self-intersections of the lines of the knot after smoothing. The points belonging to the path of the knot that has already undergone the smoothing process, i. e. for $k < i$, are all contained inside spheres of radii d_k centered around the points $\boldsymbol{x}_k$. Thus, it is safe to choose as radius d_i of the new sphere $S_{\boldsymbol{x}_i}$ $d_i = d_{\boldsymbol{x}_m \boldsymbol{x}_i} - d_m$. If $d_{\boldsymbol{x}_m \boldsymbol{x}_i} - d_m < d_{l,i}$, this setting ensures also that the sphere $S_{\boldsymbol{x}_i}$ does not contain points of the portion of the knot where there are still sharp corners, i. e. on the segments $\boldsymbol{x}_l$, $l = i+1, \ldots, N$, or on the subsegments $\boldsymbol{l}_k^0$, $k = 1, \ldots, i-1$.

can be set to be no less than d_i^*. In analogy with Eq. (5.1), we may write:

$$d_i = d_i' = \min\left\{ d_i^*, \min\left\{ \frac{l_i}{2}, \frac{l_{i+1}}{2} \right\} \right\} \tag{5.3}$$

With this choice of d_i [c], the topology of the knot is preserved after the corner in $\boldsymbol{x}_i$ is replaced with a smooth arc according to the prescription (4.6–4.7). As a matter of fact, d_i^* satisfies the condition $d_i^* \leq d_{l,i}$ ensuring that any point on the part of the knot that is unaffected by the smoothing procedure is at least at a distance $d_{l,i}$ from $\boldsymbol{x}_i$. Moreover, from Eq. (5.2) d_i^* turns out to be smaller or equal to the distance between $\boldsymbol{x}_i$ and any point of the spheres $S_{\boldsymbol{x}_k}$ that surround the regions in which the corners $\boldsymbol{x}_k$, $k = 1, \ldots, i-1$, have already been substituted. Thus, a sphere $S_{\boldsymbol{x}_i}$ of radius $d_i = d_i^*$ will certainly not contain any point of the knot apart from the subsegments $\boldsymbol{l}_i$ and $\boldsymbol{l}_{i+1}$ that are going to be substituted with a smooth arc. Finally, using the ansatz (4.6–4.7), we know that no point of that arc will be outside $S_{\boldsymbol{x}_i}$. All that is sufficient to prevent dangerous intersections of the lines of the knot that could happen after smoothing the corner in $\boldsymbol{x}_i$, so that unwanted changes of the topology of the knot are forbidden. Figure 10 provides a graphical illustration of the situation in a particular case.

[c]The exceptional case in which d_i^* will be discussed below.

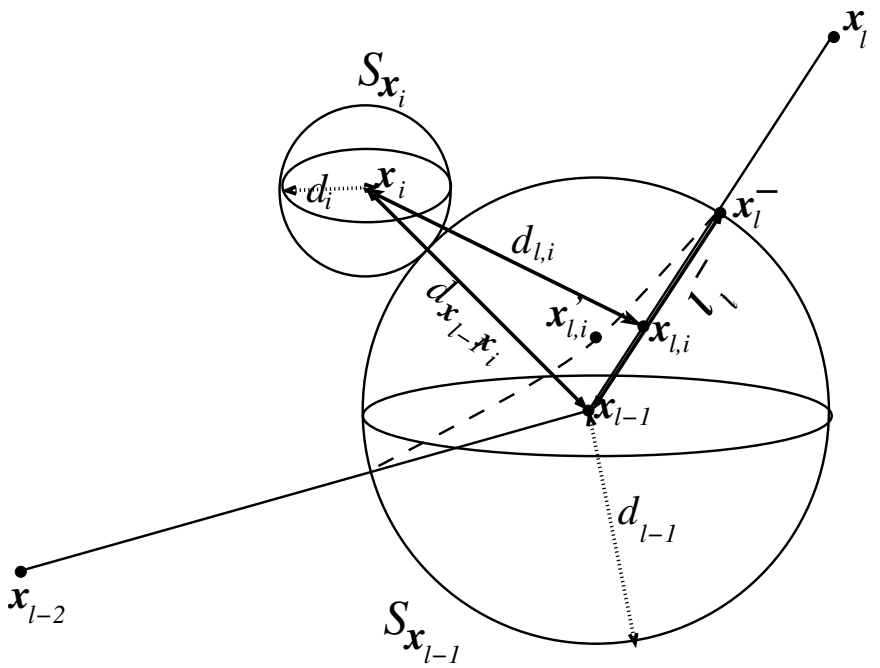

Fig. 10. In this figure we suppose that the nearest point $\boldsymbol{x}_{l,i}$ to $\boldsymbol{x}_i$ is located on the segment $\boldsymbol{l}_l$, with $l < i$. Moreover, $\boldsymbol{x}_{l,i}$ is within the distance d_{l-1} from the vertex $\boldsymbol{x}_{l-1}$. Thus, the sharp corner at $\boldsymbol{x}_{l-1}$ has been already replaced by the arcs of smooth curves $\boldsymbol{X}^+_{l-1}(S)$ and $\boldsymbol{X}^-_l(S)$ of Eqs. (4.6) and (4.7). The distance d_{l-1} is smaller by assumption than the distance $d_{\boldsymbol{x}_{l-1}\boldsymbol{x}_i}$ from $\boldsymbol{x}_i$ to $\boldsymbol{x}_{l-1}$. Moreover, $d_{l,i}$ is smaller than the distance of the point $\boldsymbol{x}_i$ to the border of any of the spheres $S_{\boldsymbol{x}_k}$ surrounding the vertices $\boldsymbol{x}_k$ for $k < i$ and $k \neq l-1$. To be safe, the radius of the sphere $S_{\boldsymbol{x}_i}$ around the point $\boldsymbol{x}_i$ is chosen to be $d_i = \min\left\{d_{\boldsymbol{x}_{l-1}\boldsymbol{x}_i} - d_{l-1}, \min\left\{\frac{l_i}{2}, \frac{l_{i+1}}{2}\right\}\right\}$.

We have still to treat the exceptional condition in which $d_i^* = 0$. Looking at the definition (5.2) of d_i^*, this implies that the center $\boldsymbol{x}_i$ of the corner to be substituted lies on the border of the sphere $S_{\boldsymbol{x}_m}$ of radius d_m centered at the point $\boldsymbol{x}_m$ for some value of $m \leq i-1$. This situation could take place only if $\boldsymbol{x}_i$ is the nearest point to $\boldsymbol{x}_m$, i. e.: $\boldsymbol{x}_i = \boldsymbol{x}_{i,m}$. After the corner centered in $\boldsymbol{x}_m$ is replaced by an arc of a smooth curve, the radius of the sphere $S_{\boldsymbol{x}_m}$ containing no other point of the knot apart from the substituted arc, could turn out to be equal to $d_m = d_{m,i}$ according to the prescription (5.3). Due to the fact that $d_{m,i}$ is also the distance between $\boldsymbol{x}_m$ and $\boldsymbol{x}_i$, the result is that the point $\boldsymbol{x}_i$ is located on the border of the sphere $S_{\boldsymbol{x}_m}$. For this reason, to prevent topology breakings after replacing the $i-$th corner that could result if $S_{\boldsymbol{x}_m}$ and $S_{\boldsymbol{x}_i}$ are overlapping, the only solution is to surround the point $\boldsymbol{x}_i$ with a sphere of radius $d_i = d_i^* = 0$. While the definition of d_i^* in Eq. (5.2) gives the correct value of d_i also in this exceptional case, this solution is of course not desirable. The recipe for overcoming this problem is very simple. First of all, the value of the old radius of the sphere $S_{\boldsymbol{x}_m}$ should be decreased together with

the portion around the corner in $\boldsymbol{x}_m$ to be replaced. For example, the new radius of $S_{\boldsymbol{x}_m}$ could be chosen as follows:

$$d_m^{new} \longrightarrow \frac{d_m^{old}}{2} \tag{5.4}$$

Next, the radius of the sphere $S_{\boldsymbol{x}_i}$ should be selected within the interval $0 < d_i < d_m^{new} = \frac{d_m^{old}}{2}$. To this purpose we have to compute once again the value of d_i^* using the formula of Eq. (5.2), which we repeat here for convenience:

$$d_i^* = \min_{k=1,\ldots,i-1} \{d_{l,i}, d_{\boldsymbol{x}_k\boldsymbol{x}_i} - d_k\} \tag{5.5}$$

The only difference between Eqs. (5.2) and (5.5) is that in Eq. (5.5) we have to take into account that, when $k = m$, the value of the radius of the sphere $S_{\boldsymbol{x}_m}$ is now d_m^{new}. At this point, we may proceed as before and choose the values d_i and d_i' using Eq. (5.3). For what it has been said before, this is sufficient to prevent unwanted topology breakings. We do not discuss here the situations in which the point $\boldsymbol{x}_i$ is located at the border of several spheres $S_{\boldsymbol{x}_m}, S_{\boldsymbol{x}_n}, \ldots$ with $m, n, \ldots < i$. In this case the new value of d_i^* computed according to Eq. (5.5) turns out to be zero because there is for instance another sphere $S_{\boldsymbol{x}_n}$ for $n < i$ and $n \neq m$ such that $d_{\boldsymbol{x}_n\boldsymbol{x}_i} - d_n = 0$. This situation can be easily tackled by rescaling the radius d_n of $S_{\boldsymbol{x}_n}$ using Eq. (5.4) with the index n instead of m. After that, it is possible to compute the new value of d_i^* applying Eq. (5.5). The final radius of the sphere $S_{\boldsymbol{x}_i}$ will be given once again by Eq. (5.3).

Summarizing, in this Section an algorithm has been provided in order to prevent during the smoothing procedure of a knot unwanted breakings of its topology following undesired self-intersections of its path. An example of curve describing a discrete knot 3_1 off-lattice before and after the smoothing procedure is shown in Fig. 11. The algorithm is relatively straightforward despite the fact that we are con-

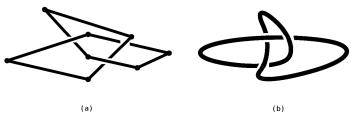

Fig. 11. A knot 3_1 with minimal length defined off-lattice (a) before and (b) after the smoothing procedure.

sidering here very general discrete knots consisting of segments of different lengths and defined both off- or on-lattice. The idea behind the algorithm is simple. It consist in enclosing each part of the knot where a sharp corner has been substituted with an imaginary sphere whose radius is choosen is such a way that there are no overlaps between different spheres or between a sphere and the part of the knot that is unaffected by smoothing. This is sufficient in order to avoid topology breakings and self-intersections. Of course in off-lattice calculations, where the segments

are allowed to get arbitrarily close to each other, the radii d_i of the spheres $S_{\boldsymbol{x}_i}$, $i = 1, \ldots, N$, and thus the portions of the corners that have been replaced, could become smaller and smaller when the value of i increases. As explained in Point 4 on page 15, in the case in which the arcs replacing the sharp corners are confined just in a tiny portion of the knot, a more extensive Monte Carlo sampling could be necessary in order to evaluate with a good approximation the multiple curvilinear integrals that characterize the expressions of numerical knot invariants. This is a drawback, but it cannot be avoided by any prescription in the case of off-lattice calculations.

6. Speeding up the smoothing algorithm and the Monte Carlo computation of the Vassilieve knot invariant of degree 2

The smoothing algorithm and the prescriptions for preserving the topology of the knot during smoothing have been worked out in Sections 4 and 5 in the most general case. In more particular cases several simplifications are possible.

First of all, the parametric equations of the arcs of a smooth curve that replace the sharp corners given in Eqs. (4.6–4.7) considerably simplify if we assume that all segments composing the knot have the same length and the lengths d_i of the subsegments $\boldsymbol{l}_i^+$ coincide with the lengths d_i' of the subsegments $\boldsymbol{l}_{i+1}^-$. This is true both on- and off-lattice. On a lattice it is also possible to define a fixed minimal distance d such that, if all the spheres $S_{\boldsymbol{x}_i}$ will have radii $d_i \leq d$, the topology of the knot will be automatically preserved without the need of the prescriptions of Section 5. For instance, on a simple cubic lattice one may always choose $d_i = d_i' = \frac{l_i}{2}$. In this case Eqs. (4.6–4.7) reduce to the equation:

$$\boldsymbol{X}_i^{\pm}(S) = \left(1 - \sin\left(\theta_0^{\pm}(S)\right)\right) \boldsymbol{l}_i^+ + \left(1 - \cos\left(\theta_0^{\pm}(S)\right)\right) \boldsymbol{l}_{i+1}^- + \boldsymbol{x}_i \tag{6.1}$$

where

$$\theta_0^+(S) = \left(S - [S] - \frac{1}{2}\right) \frac{\pi}{2} \tag{6.2}$$

and

$$\theta_0^-(S) = \left(S - [S] + \frac{1}{2}\right) \frac{\pi}{2} \tag{6.3}$$

Let's now consider more in detail the computation of numerical knot invariants (NKIs). The example of the Vassiliev invariant of degree 2 $\varrho(C)$ will be used to fix the ideas. Monte Carlo methods are much more convenient than traditional numerical techniques in calculating the values of NKIs. For instance, in order to evaluate $\varrho(C)$ with sufficient precision in the case of knots of length $L \leq 120$, a few millions of sampling points are enough. This is a quite good performance if we take into account that for $N = 120$, the total volume that has to be checked, defined by Eq. (3.13) and discussed in the related comments, is of the order $\frac{120^4}{24} \sim 9 \cdot 10^6$. Monte Carlo algorithms offer also the advantage that the sampling procedure can

be easily parallelized on a computer. Still, the numerical evaluation of a NKI could become challenging if a very high precision is required to determine the value of that NKI or the number of segments N composing the knot is large. In those cases, it is highly advisable to adopt strategies that are able to reduce the calculation time. NKIs have a very nice feature in this respect, namely their values are discrete. This is very useful in concrete numerical simulations, where the main role of knot invariants is to make assessments on the a priori unknown topological configuration of a knot. To this purpose, it is not necessary to evaluate an NKI with an arbitrary high precision. This point is well illustrated by the example of the second Vassiliev knot invariant of degree 2. If two knots C and C' can be distinguished by $\varrho(C)$, i. e. $\varrho(C) \neq \varrho(C')$[d], then the condition

$$|\varrho(C) - \varrho(C')| \geq 2 \tag{6.4}$$

is always satisfied. As a consequence, in order to ascertain if two knots are topologically inequivalent according to $\varrho(C)$, it is not necessary that the standard deviation σ of the numerical calculation of $\varrho(C)$ defined in Eq. (3.17) will be as low as possible. It is sufficient to require that the value of σ remains below a given threshold $\sigma_{threshold}$. For instance, if we choose:

$$\sigma_{threshold} = \frac{1}{6.11} \sim 0.16 \tag{6.5}$$

and $\sigma \leq \sigma_{threshold}$, the probability that the Monte Carlo evaluation of $\varrho(C)$ gives a result within an error of ± 1 or greater is of the order $1 \cdot 10^{-9}$, meaning that this event is very unlikely to occur. As an example, in order to ascertain if the topology of a knot 4_1 has been modified during the sampling process by a random transformation of its path, we set $\sigma_{threshold} = 0.3$. To see why this choice is safe, we recall that for a 4_1 knot the exact value of $\varrho(C)$ is approximately $\varrho(4_1) \sim -2.08$. Moreover, a close inspection of billions of random conformations obtained from the performed simulations has shown that a knot may relatively easily decay into a knot of simpler topology according to the Rolfsen table. The passage to a knot of higher topological complexity after a random transformation is instead a rare event, whose probability decreases with the increasing of the degree of complexity. The only knots that are topologically simpler than 4_1 are the unknot 0_1 and the trefoil 3_1. The second Vassiliev invariant of degree 2 of these knots is $\varrho(0_1) \sim -0.08$ and $\varrho(3_1) = 1.91$ respectively. Both these values are far from that of the knot 4_1, for which $\varrho(4.1) \sim -2.08$. As a consequence, a threshold standard deviation of 0.3 is more than enough to prevent the change of the knot type from 4_1 to 3_1 or to

[d] We recall here that there exists no knot invariant that is able to distinguish unambiguously all different types of knots. The second Vassiliev invariant of degree 2 is not an exception to this rule. Indeed, there are many knots for which the second coefficient of the Conway polynomial $a_2(C)$ is the same. This implies that $\varrho(C)$, which is related to $a_2(C)$ by Eq. (2.10), can at most be used to distinguish classes of knots having different values of $a_2(C)$. Still, $\varrho(C)$ may be considered as a relatively powerful knot invariant. For example, it is able to distinguish uniquely the knots 9_1 and 10_3 from all other knots up to ten crossings.

0_1. Passages from a knot 4_1 to a knot with a higher topological complexity are extremely rare, but cannot be excluded. Yet, even if this situation will occur, most of the knots up to eight crossings have values of $\varrho(C)$ that are not equal to $\varrho(4_1)$. For this reason, if $\sigma = \sigma_{threshold} = 0.3$, it is not very likely that the topology of a knot 4_1 could be confused with that of one of those other knots during the Monte Carlo sampling procedure of Eqs. (3.14) and (3.16). Of course, as already mentioned, there is no topological invariant that is able to distinguish unambiguously a knot from the other. For instance, the value of $\varrho(C)$ of the knots $6_2, 7_7, 8_5, 8_{11}$ and 8_{17} coincides with that of the knot 4_1. If a change of topology from 4_1 to any of these knots will take place, there will almost be no way [e] to detect it using $\varrho(C)$ and the introduction of additional knot invariants is needed. Despite these limitations, the invariant $\varrho(C)$ can be successfully applied to preserve the topology during numerical simulation for several knots like $0_1, 3_1, 4_1, 5_1, 5_2, 7_1, 7_3, 8_3, 8_{19}, 9_1, 10_3$. In fact, the values of $\varrho(C)$ of all these knots are not encountered in topologically simpler knots and, as already mentioned, the accidental transformation to knots with higher topological complexity in the aftermath of a random transformation is an extremely rare event. For simulation purposes, the fact that there is no need to push the precision below a threshold such as that in Eq. (6.5) is very helpful to avoid a consistent increase of the calculation times. Indeed, the time τ necessary for computing $\varrho(C)$ scales linearly with the number of samples n, but an increasing of n by a factor $\lambda > 1$ produces an improvement of σ only by a factor $\frac{1}{\sqrt{\lambda}}$, i. e. $\sigma \longrightarrow \frac{\sigma}{\sqrt{\lambda}}$. We have checked that this scaling law, that is predicted in the case of gaussian distributions, is actually verified in our simulations.

Besides the level of precision, another important factor that determines the computation time τ is the number N of segments (or equivalently the number of arcs of G^1-curves) composing the knot. We stress the fact that τ depends on the total number of segments N of a knot and not on its total length L. In the opposite case, τ could be reduced arbitrarily. To this purpose it would be sufficient to rescale the lengths l_i of the N segments composing a given knot C by an arbitrarily small factor $\eta << 1$:

$$l_i \longrightarrow l'_i = \eta l_i \qquad\qquad i = 1, \ldots, N \tag{6.6}$$

With this procedure the new knot C' with segments of lengths $l'_1, \ldots, l'_N$ becomes just a smaller copy of the old knot C. Its topology remains however the same as that of C. As a consequence, the results of the evaluation of any numerical knot invariant for C and C' will coincide as expected. Unfortunately, this means also that the passage from the knot C to C' will not be helpful to speed up the calculation of an NKI. The reason is that the form of the curvilinear integrals appearing in the expressions of numerical topological invariants does not change when passing from

[e]The patterns in which different knots decay to simpler topologies during a simulation are different for different knots. This fact provides a further way to check if, at some stage of the random sampling, a knot C has been transformed into a knot C' of higher or lower topological complexity, though they cannot be distinguished using a given NKI.

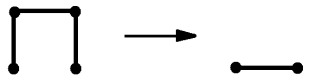

Fig. 12. Reduction to a single segment of an element of the discrete knot composed by three consecutive segments such that its ends are at a distance equal to the unit size on a simple cubic lattice. The topology of the knot is not affected by this reduction.

C to C'. In particular, the dependence on the parameter η simply disappears due to the fact that NKIs, like all topological invariants, are unaffected by rescalings. A quantity that is able to distinguish two knots that just differ by their size cannot be a topological invariant. For instance, it is easy to check that $\varrho(C)$ is a scale invariant quantity.

Following the above reasoning, a good strategy to increase the speed of the calculation of an NKI consists in decreasing the number of segments composing the knot. To this purpose, a few procedures that apply to discrete knots is proposed below.

(1) For a general discrete knot, two or more contiguous segments of lengths $l_i, l_{i+1}, \ldots, l_{i+k}$ with $2 \leq k < N$ that have all the same direction can be put together in a single segment of length $l_i + l_{i+1} + \ldots l_{i+k}$. In this way the number of segments is reduced from N to $N - k + 1$.
(2) On a simple cubic lattice, configurations of three segments whose starting and ending points are at a distance of one lattice size can be easily substituted by one segment as shown in Fig. 12. This reduces the length of the knot by two segments every time such configurations are encountered.
(3) Always on a simple cubic lattice it is possible to group together two or three contiguous segments in a single one, see Figs. 13 (a) and (b) and 14 (a), (c–e). On triangular lattices further reductions are allowed, see for instance Fig. 14 (b). We note that the first substitution in Fig. 14 can cause intersections between two segments after the grouping and should be treated with some care.

Other algorithms to decrease the size of a knot can be found in Refs. [41] and [42].

In the rest of this Section a method will be presented for speeding up the Monte Carlo procedure in the special case in which the numerical knot invariants are just needed to check the possibility of a topology change in a knot after a random transformation, but it is not necessary to ascertain the exact type of the knot. To fix the ideas, we will consider the specific case of $\varrho(C)$ and imagine that the random transformation involves K contiguous segments, where $0 \leq K \leq N$. Let's suppose that C_R is the polymer conformation before the transformation. The goal is to ascertain if C_T, i. e. the new knot conformation obtained after the random transformation, is still topologically equivalent to C_R or not. Instead of computing the whole knot invariant $\varrho(C)$, it is much better to evaluate the difference $\Delta\varrho(C) = \varrho(C_T) - \varrho(C_R)$.

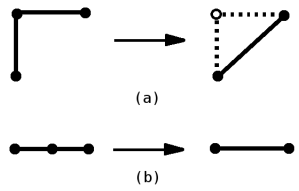

Fig. 13. This figure displays the possible configurations on a simple cubic lattice of two contiguous segments and their substitution with a single segment. The topology of the knot is left unchanged after the substitution.

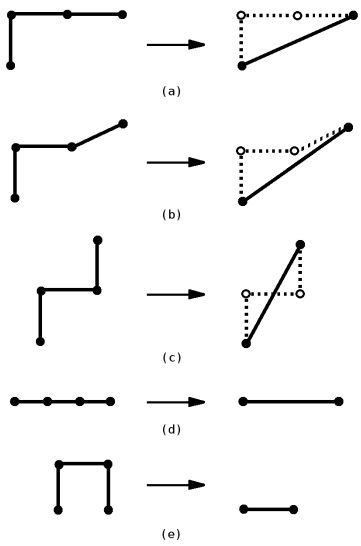

Fig. 14. Panels (a) and (c-e) display the possible configurations on a cubic lattice of three contiguous segments that can be substituted with a single segment. Panel (b) is an example of segment reduction on a triangular lattice

Clearly, if $\varrho(C)$ could distinguish unambiguously any two topologically different knots, C_R and C_T would be equivalent if and only if $\varrho(C_T) - \varrho(C_R) = 0$. Unfortunately this is not the case, but, as discussed after Eq. (6.5), the second Vassiliev invariant of degree 2 is powerful enough to be applied in order to detect with a very high precision the changes of topology of many knots. Thus, for knots like the already mentioned $0_1, 3_1, 4_1, 5_1, 5_2, 7_1, 7_3, 8_3, 8_{19}, 9_1, 10_3$, we expect that the condition $\Delta\varrho(C) = \varrho(C_T) - \varrho(C_R) \sim 0$ is sufficient to conclude if the topology of C_T coincides with that of C_R or not. The advantage of considering $\Delta\varrho(C)$ instead of computing the value of the knot invariant for C_T is that in this way we subtract

from the calculation the part of the knot that has remained unchanged after the transformation.

To realize how this strategy is working, we consider the calculation of $\varrho_2(C)$, which, as it possible to see from Eq. (2.3), is the contribution to $\varrho(C)$ that requires the greatest computational effort. From Eq. (3.13) it turns out that the volume that the Monte Carlo sampling procedure has to explore to estimate the value of $\varrho_2(C)$ is equal to $N^4/24$. If the number of the changed segments is K, then the part of the volume containing only segments that have not been affected by the transformation is equal to $(N-K)^4/24$. As a consequence, in first approximation, the effective volume to be taken into account in the evaluation of the difference $\varrho(C_T) - \varrho(C_R)$ is

$$\begin{aligned} S_K &= \frac{N^4}{24} - \frac{(N-K)^4}{24} \\ &= \frac{NK^3}{6} - \frac{N^2K^2}{4} + \frac{N^3K}{6} - \frac{K^4}{24} \end{aligned} \tag{6.7}$$

Clearly, the minimum of S_K with respect to K occurs when $K = 4$ (we do not consider here transformations with less than 4 segments). Due to the fact that the derivative of S_K with respect to K in the range $0 \leq K \leq N$ is always positive, because $\frac{dS_K}{dK} = \frac{(N-K)^3}{6} > 0$, it turns out that S_K grows with K until it reaches its maximum when $K = N$ (transformations of more than N segments do not make sense). If K is small with respect to N, Eq. (6.7) shows that the volume to be explored in the computation of $\Delta\rho_2(C)$ is much less than that needed to obtain $\varrho_2(C)$. For instance, when $K = N/5$, we obtain:

$$S_K = 0.5904 \times \frac{N^4}{24} \tag{6.8}$$

so that only 60% of the original volume $\frac{N^4}{24}$ should be considered. In the best case, $K = 4$, instead,

$$S_4 \sim \frac{2N^3}{3} \tag{6.9}$$

which implies an enormous gain in speed.

7. An application: cooling and compression of long polymer rings in knotted configurations

The algorithms discussed in the previous Sections will be applied here to numerical simulations of physical systems in which topology plays a relevant role. Examples of such systems can be found everywhere in nature, for instance in the DNA [1,43, 44,45,47], in superfluids [48] and in the solar magnetosphere [49]. Knotted polymer rings can also be synthesized [50,51]. In this Section an application in polymer physics will be presented.

Before starting, we have still to provide a concrete sampling prescription for evaluating the numerical knot invariants with the Monte Carlo recipe given in

Section 3. We suppose that the discrete knot has already undergone the smoothing precedure of Sections 4 and 5. After the sharp corners have been replaced by smooth arcs that are confined inside the spheres $S_{\boldsymbol{x}_i}$ of radii d_i, d_i' chosen in such a way to prevent topology breakings, the points on the knot are sampled with the following strategy:

Step 1 Pick up a real random number ξ_1 in the interval $[0, N]$. This random variable identifies the portion of the knot that corresponds to the segment $\boldsymbol{l}_i$ before smoothing with $i = [\xi_1] + 1$. For example, using the notations of Eqs (3.5–3.6), $\xi_1 = S$ and the end points of the segment $\boldsymbol{l}_i$ are given by $\boldsymbol{x}_i = \boldsymbol{X}([S] + 1)$ and $\boldsymbol{x}_{i-1} = \boldsymbol{X}([S])$. These formulas may be used also in the special case $i = 1$, see Eq. (3.6), provided the point $\boldsymbol{x}_0$ is identified with $\boldsymbol{x}_N$. Next, we have to choose randomly also $\xi_2, \ldots, \xi_{m^{(z)}}$ within the ranges $[0, \xi_1], \ldots, [0, \xi_{(m^{(z)}-1)}]$, see Eq. (3.15). Considering the case of $\varrho(C)$ to fix the ideas, we have that $z = 1, 2$ and $m^{(1)} = 3$, $m^{(2)} = 4$. The three parameters necessary to compute the integral $\varrho_1(C)$ of Eq. (2.2) are $\xi_1 = S$, $\xi_2 = T$ and $\xi_3 = U$. The second integral $\varrho_2(C)$ of Eq. (2.3) requires to randomly choose four variables: $\xi_1 = S$, $\xi_2 = T$, $\xi_3 = U$ and $\xi_4 = V$.

Step 2 We assume that the knot is oriented in such a way that the $i-$th segment $\boldsymbol{l}_i$ is coming before the segment $\boldsymbol{l}_{i+1}$. In this step we check if one of the following three conditions are satisfied:

$$0 \leq S - [S] < \frac{d_{i-1}'}{l_i} \tag{7.1}$$

$$\frac{d_{i-1}'}{l_i} \leq S - [S] < \frac{l_i - d_i}{l_i} \tag{7.2}$$

$$\frac{l_i - d_i}{l_i} \leq S - [S] < 1 \tag{7.3}$$

The first condition (7.1) identifies the subsegment $\boldsymbol{l}_i^-$, the second condition (7.2) the subsegment $\boldsymbol{l}_i^0$ and the third one (7.3) the subsegment $\boldsymbol{l}_i^+$.

Step 3 When condition (7.1) is fulfilled, verify if the relation

$$\frac{\boldsymbol{l}_{i-1}^+ \cdot \boldsymbol{l}_i^-}{l_{i-1}^+ l_i^-} = -1 \tag{7.4}$$

is satisfied[f]. If yes, the segments $\boldsymbol{l}_{i-1}^+$ and $\boldsymbol{l}_i^-$ around the corner $\boldsymbol{x}_{i-1}$ are antiparallel. This means that $\boldsymbol{l}_{i-1}^+$ and $\boldsymbol{l}_i^-$ do not form a sharp corner in $\boldsymbol{x}_{i-n}$, so that they have not been replaced during the smoothing procedure. As a consequence, the parametrization of the knot given in Eqs. (3.5–3.6) is still valid. If instead the segments $\boldsymbol{l}_{i-1}^+$ and $\boldsymbol{l}_i^-$ are not antiparallel, then we have to use for $\boldsymbol{l}_i^-$ the parametrization of the arc of smooth curve given in Eq. (4.7) after

[f]By construction the contiguous subsegments $\boldsymbol{l}_{i-1}^+$ and $\boldsymbol{l}_i^-$ are oriented in such a way that they are antiparallel when they form an angle of 180°, see Fig. 5.

n	$\varrho(C)$
10^6	1.9096 ± 0.0991
10^7	1.9179 ± 0.0326
10^8	1.9170 ± 0.0095
10^9	1.9168 ± 0.0032

Table 1. Computation of the knot invariant $\varrho(C)$ for the knot 3_1 with 24 segments on a simple cubic lattice. The results of the numerical calculation of $\varrho(C)$ are displayed for different values of the number of samples n used in the Monte Carlo integral procedure. As it can be seen, by gradually increasing n, the numerical values of $\varrho(C)$ asymptotically approach the exact value of the Vassiliev knot invariant of degree 2 which, in the case of the knot 3_1, is approximately equal to 1.9167.

replacing i with $i-1$. We remark in fact that we are dealing here with the subsegment $\boldsymbol{l}_i^-$ corresponding to the corner $\boldsymbol{x}_{i-1}$, while Eq. (4.7) refers to the next corner $\boldsymbol{x}_i$. In practice, using Eq. (4.7), the point corresponding to the parameter $\xi_1 = S$ is projected onto the point $\boldsymbol{X}_i^-(S)$ lying on the arc of smooth curve that has replaced the sharp corner. A similar procedure is adopted when condition (7.3) is true. In that case the condition of being antiparallel is concerning the segments $\boldsymbol{l}_i^+$ and $\boldsymbol{l}_{i+1}^-$:

$$\frac{\boldsymbol{l}_i^+ \cdot \boldsymbol{l}_{i+1}^-}{l_i^+ l_{i+1}^-} = -1 \tag{7.5}$$

If it turns out that $\boldsymbol{l}_i^+$ and $\boldsymbol{l}_{i+1}^-$ are not antiparallel, then the point $\boldsymbol{X}(S)$ should be mapped on the smoothed knot using Eq. (4.6). Finally, if condition (7.2) is satisfied, we are on the subsegment $\boldsymbol{l}_i^0$, thus in a part that has not been affected by smoothing. As a consequence, for the values of $\xi_1 = S$ in the interval $[\frac{d'_{i-1}}{l_i}, \frac{l_i - d_i}{l_i}]$, it is possible to apply the old parametrization of Eqs. (3.5–3.6). Steps 2 and 3 should be repeated for $\xi_2 = T$, $\xi_3 = U$ etc.

After having sampled the first set of points $\xi_1^{(1)}, \ldots, \xi_{m^{(z)}}^{(1)}$, with $z = 1, 2, \ldots$ according to the above prescriptions, we have to repeat the procedure for $\nu = 2, \ldots, n$.

We are now ready to compute numerical knot invariants with the smoothing procedure of Sections 4, 5 and the Monte Carlo algorithm of Section 3. As a test, we will calculate the value of the Vassiliev invariant of degree 2 $\varrho(C)$ of different knots and lengths. All knots are originally defined on a simple cubic lattice, but after the reduction of the number of segments discussed in Section 6 this is no longer true. Our Monte Carlo calculations show that the obtained values of $\varrho(C)$ approach the exact value of this invariant with a precision that increases with the number of sampled points n. In Table 1 we report for instance the case of a knot 3_1 with 24 segments. Table 2 illustrates how the presence of the sharp corners affects the calculations of $\varrho(C)$. In the second column of Table 2, the exact value $\varrho_a(C)$ of the Vassiliev knot invariant of degree 2 is provided for several knots with $N = 90$ segments. Within the given errors, the values $\varrho_{sp}(C)$ obtained by Monte

knot type	$\varrho_a(C)$	$\varrho_{sp}(C)$	$\varrho_{ns}(C)$	n_{sc}
0_1	$-\frac{1}{12}$	-0.0839 ± 0.0332	$+0.5526 \pm 0.0569$	77
3_1	$+\frac{23}{12}$	$+1.9170 \pm 0.0553$	$+2.4781 \pm 0.0465$	68
4_1	$-\frac{25}{12}$	-2.0847 ± 0.0533	-1.5214 ± 0.0845	68
5_1	$+\frac{71}{12}$	$+5.9174 \pm 0.0653$	$+6.4523 \pm 0.0845$	65
6_1	$-\frac{49}{12}$	-4.0856 ± 0.0723	-3.5717 ± 0.1007	62
7_1	$+\frac{143}{12}$	$+11.9173 \pm 0.0652$	$+12.4258 \pm 0.1217$	62
8_1	$-\frac{73}{12}$	-6.0822 ± 0.0529	-5.6380 ± 0.0774	54
9_1	$+\frac{239}{12}$	$+19.9158 \pm 0.0855$	$+20.4041 \pm 0.1579$	59

Table 2. This table provides the values of the Vassiliev knot invariant of degree 2 for the knots 0_1, 3_1, 4_1, 5_1, 6_1, 7_1, 8_1 and 9_1. $\varrho_a(C)$ denotes the exact value of the knot invariant. $\varrho_{sp}(C)$ refers to the results of the computation of the knot invariant obtained after performing the smoothing procedure described in Section 4. $\varrho_{ns}(C)$ is instead the value of the knot invariant derived without the smoothing procedure. The data of $\varrho_{sp}(C)$ and $\varrho_{ns}(C)$ have been computed using the same number of samples, which varies depending on the kind of knot. Finally, n_{sc} is the number of sharp corners contained in the knot before the smoothing procedure.

Carlo integration after the smoothing procedure (sp) are in agreement with the exact values, see the third column of Table 2. We are also reporting the results of the calculations performed without the smoothing procedure, see the values of $\varrho_{ns}(C)$ in the fourth column of Table 2. The differences between $\varrho_{sp}(C)$ and $\varrho_{ns}(C)$ show that the presence of sharp corners in the case of discrete knots does not allow the correct evaluation of the knot invariant $\varrho(C)$.

Finally, we apply the previously developed algorithms to a concrete simulation with the aim of exploring the energy landscape of a single knotted polymer ring. The monomers of the polymer are subjected to very short-range interactions which are attractive or repulsive, corresponding to poor or good solutions [52,53]. The knots are defined on a simple cubic lattice and the sampling of the polymer conformations is performed using a variant of the Wang-Landau Monte Carlo algorithm [54]. The Vassiliev knot invariant of degree 2 $\varrho(C)$ is used in order to detect changes in the topology during the random generation of the conformations to be sampled. The Wang-Landau algorithm performs the sampling in the microcanonical ensemble. It delivers the so-called density of states $\Omega(E)$ as a function of the energy E. The possible energy values are given by $E = m\epsilon_0$, where ϵ_0 is a constant and $m = 1, 2, \ldots$ denotes the number of contacts [55,56]. A contact occurs when the distance between two points of the knot that are not contiguous is equal to one lattice unit. Each contact has a fixed energy cost that, depending if the interactions are attractive or repulsive, can be negative ($\epsilon_0 < 0$) or positive $\epsilon_0 > 0$. From now on we assume that the interactions are attractive, so that higher values of m correspond to lower energies. In the following, it will be also convenient to consider the number of contacts m instead of the energy E. All details about the Wang-Landau algorithm, the interactions used and the whole setup can be found in Ref. [29].

The model depicted above is simple, but sufficient to capture many features of polymers in poor of good solutions. Once the density of states $\Omega(E)$ is known, it is straightforward to compute the expectation values of the observables in the canonical ensemble for any range of temperatures, see [29,56] for a concise review on Wang-Landau based techniques applied to polymers. This is undoubtely an advantage with respect to traditional Monte Carlo techniques. The price to be paid is that the derivation of $\Omega(E)$ is computationally demanding in the case of polymers subjected to topological constraints. In order to consider the whole energy spectrum, in fact, it is necessary to sample also knot conformations that are extremely rare. The latter are usually conformations near the minimum of the energy spectrum and are physically relevant when studying the phase diagram of polymer knots. Unfortunately, the computation of the density of states together with the requirement that the topology should be preserved during the sampling process becomes a challenging problem for long knots consisting of a number $N > 1000$ of segments.

Here a simpler task than the computation of the density of states will be considered, namely we are interested to explore the energy landscape of knotted polymer rings. This problem has been tackled first exploiting the alternative method of [56] in order to preserve the topology of the knot. This method is very fast, but is restricted by the fact that at each step of the sampling process at most only four segments can be randomly changed. Despite the simplicity of the model discussed before, it turns out that the energy landscape of very long knots subjected to attractive short-range interactions is non-trivial. The calculations made so far suggest that its structure could be that of a funnel. For instance, Fig. 15 shows the histogram counting how many conformations of a knot 3_1 with $N = 4320$ have been visited during a run that started from a seed with $m = 0$ contacts and has been stopped after a conformation with $m = 4395$ was reached. As it is possible to see from that figure, the code spends a considerable amount of time to sample the most probable energy domain in which $0 \leq m \leq 1500$. Hundreds of billions of conformations should be sampled before knots conformations with contact numbers $m > 1500$ are detected. In the range $1500 \leq m \leq 4395$ it is possible to recognize five different regions, see the inset of Fig. 15. The sampling process seems to be trapped successively in one of these regions until the next region with lower values of m is found. All that is reminding the multi-funnel structure of the energy landscape of proteins in which relative energy minima are confined in narrow funnels inside of which even narrower funnels with lower minima are located. A possible explanation of this structure is that conformations with large contact numbers are very compact, while statistically the majority of conformations is swollen. For that reason, it is necessary to sample many conformations before those with small gyration radii are detected. Yet, the appearance of regions with different scales of the gyration radius is somewhat surprising. In addition, there are also conformations whose shapes are very stable and are persisting after billions of random transformations. This is the case of semi-crystallized conformations like that shown in Fig. 16. The glance into

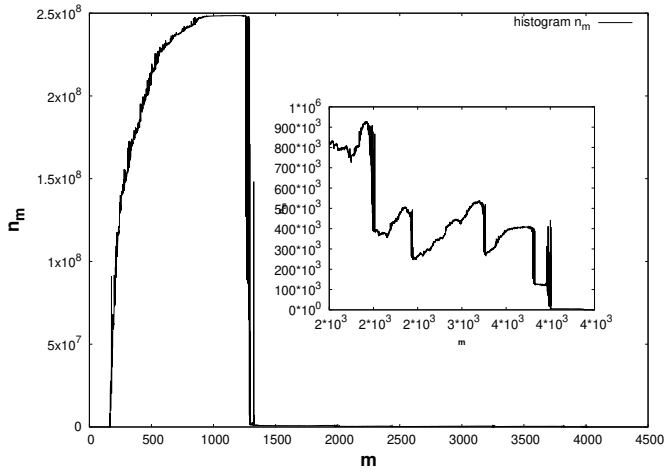

Fig. 15. Histogram showing how many times n_m a conformation of energy m has been sampled while exploring the energy landscape of a knot 3_1 with $N = 4320$ segments in the range $0 \leq m \leq 4395$. Inset: details of the histogram in the range $1500 \leq m \leq 4500$.

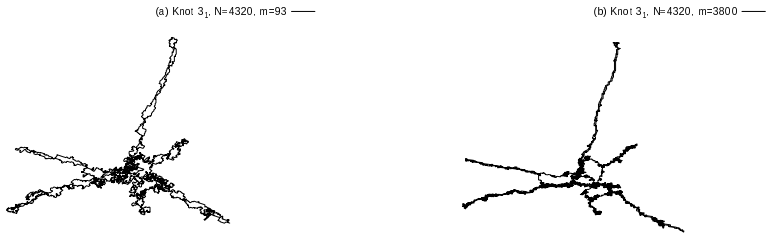

Fig. 16. This figure shows two semi-crystallized conformations of the same knot 3_1 with $N = 4320$ randomly generated at different steps during the sampling. In conformation (a) the number of contacts is $m = 93$, while in conformation (b) $m = 3800$. In both case the shape is characterized by a main body with four rings from which six long arms are departing. This shape has been preserved during the billions of random transformations needed to obtain (b) from (a).

the complexity of long polymer knots presented above has been obtained using the approach of Ref. [56] in which the detection of possible breakings of the topology of a knot during sampling is very fast. The main drawback of that approach, as already mentioned, is that the changes between the next knot conformation to be accepted or rejected and the previous one are limited to a tiny portion of the loop. This drawback slows down the process of searching the conformations of minimum energy of a knotted polymer ring, i. e. those with the maximum number of contacts according to our settings. For instance, a set of about $9 \cdot 10^{11}$ conformations had to

be generated before arriving at the ultra-compact knot 9_1 with $N = 3994$ segments displayed in Fig. 1. Despite the high speed of the algorithm [56] for preserving the topology of the knot, almost one year of calculations on a modern workstation with 48 cores have been necessary for that.

The strategy followed here is to use an alternative method based on the Vassiliev knot invariant of degree 2 $\varrho(C)$. This allows to change within a single random transformation an arbitrary number of segments in the loop. In order to calculate $\varrho(C)$, the Monte Carlo algorithm of Section 3 has been applied together with the smoothing procedures of Sections 4 and 5. The minimal number n of points to be sampled to compute the integrals (2.2) and (2.3), see also Eq. (3.14) for the definition of n, depends on the value of the threshold standard deviation $\sigma_{threshold}$ defined in Eq. (6.5) and on how complicated is the conformation whose topology should be detected. For instance, in the case of the knot 9_1 with $N = 500$ that will be considered here, we have found that a convenient choice to ensure that the topology is detected without errors is $\sigma_{threshold} \sim 1.3$. Concerning the complexity of the conformation, as a general rule discrete knots with a lot of bendings need a higher value of n than knots whose path is less bended. In a single simulation n may oscillate within a wide interval. For this reason, in order to save computational time, our code has been designed in such a way that it is able to determine automatically the optimal number of the points to be sampled. While a given simulation is running, the value of $\varrho(C)$ calculated with the Monte Carlo integration of Section 3 is stored for each accepted conformation together with the standard deviation σ obtained using Eq. (3.17). These data show that σ steadily varies within the interval $0 < \sigma < \sigma_{threshold}$ depending on the given conformation and on n. The fact that σ randomly increases or decreases while the knot conformations randomly change provides a good method to check if the topology of the knot is preserved. It is sufficient to monitor the conformations for which σ is very small. For example, the knot 9_1 has the highest value of $\varrho(C)$ within all knots up to ten crossings: $\varrho(9_1) = 20 - \frac{1}{12}$. Only 9_3 and 10_{139} have values of $\varrho(C)$ that are comparable: $\varrho(9_3) = \varrho(10_{139}) = 18 - \frac{1}{12}$. If at every stage of a simulation there are accepted conformations for which the computed value of $\varrho(C)$ is very near to the true value $\varrho(9_1) = 20 - \frac{1}{12}$ and the standard deviation of the calculation is very low, this only means that it is very unlikely that the original topology of the knot 9_1 has changed. By checking also the values of $\varrho(C)$ and σ of the conformations that have been rejected, one may observe how a given knot decays into other knots after a random transformation. Since different knots have different decay patterns, it is possible to assess if a knot has decayed into a simpler knot with the same value of $\varrho(C)$ or not.

The Monte Carlo evaluation of $\varrho(C)$ requires to sample a large number of points n. For the aforementioned 9_1 knot with $N = 500$ and $\sigma_{threshold} \sim 1.3$, the values of n depend on how a conformation is complicated and range within the interval $10^6 \leq n \leq 4.2 \cdot 10^9$. The resulting heavy computational workload has been tackled by increasing the degree of parallelisation of the code and using GPUs. Moreover,

in order to speed up the computations, several of the methods explained in Section 6 have been exploited. Particularly efficient for this purpose turn out to be the procedures that reduce the number of segments mentioned in point 3 on page 26. A further gain of speed has been obtained introducing compression during the sampling of the knot conformations. This means that a new knot conformation is accepted if it fulfills the Wang-Landau acceptance criterion and its gyration radius is equal or smaller than that of the previous conformation [g]. Compression eases the search of the ultra low energy conformations because they are ultracompact.

The conformation used as a seed in our simulations of an 9_1 knot with $N = 500$ segments, see Fig. 17, plot with thinner lines, has contact number $m = 110$ and gyration radius (measured in lattice units) $R_G \sim 107.00$. This is actually a non trivial conformation that has been obtained acting with millions of random transformations on a simpler conformation. As mentioned before, the complexity of a conformation is measured here by taking into account the number of points n to be sampled in order to evaluate $\varrho(C)$ with a standard deviation $\sigma \leq \sigma_{threshold}$. The seed requires $n \geq 1.4 \cdot 10^7$, which is quite a high value. Starting from the seed, each new conformations is generated by random transformations affecting portions of the loop whose lengths range within five and fifteen segments. The results of the simulation are summarized by the histogram in Fig. 18-(a), in which the number n_m of visited conformations with contact number m is counted[h]. As it is possible to see, after sampling about $1.4 \cdot 10^6$ knot conformations the energy range $45 \leq m \leq 676$ has been explored. The compression criterion forbids to attain contact numbers such that $m < 45$. The conformations that have been found at the lower bound of the energy range ($m = 676$) have a gyration radius of $R_G \sim 17,57$ in lattice units. An additional number of $1.0 \cdot 10^6$ conformations has been sampled without detecting any conformation with $m > 676$ before the simulation has been stopped[i].

The same simulation has been repeated using the algorithm of Ref. [56] in order to preserve the topology of the knot. During a time comparable to that of the previous simulation, the histogram of Fig. 18-(b) has been produced. Clearly, a much larger number of conformations have been visited with respect to the method based on the Vassiliev knot invariant of degree 2. However, the fact that only four segments can be changed by a single random transformation is a disadvantage in this case. Indeed, the knot remains trapped within a small set of conformations with contact numbers in the interval $101 < m < 223$. Of course, this does not

[g] Apart from compression, it is also possible to apply cooling. In this case, during the sampling a new knot conformation is accepted only if it fulfills the Wang-Landau acceptance criterion and its energy is equal or lower than that of the previous conformation. Cooling much more likely than compression produces frozen conformations like those of Fig. 16.

[h] Let us note that the histogram of Fig. 18-(a) confirms the possibility of a funnel structure of the energy landscape of polymer knots. Like in Fig. 15, in fact, this histogram presents plateaux corresponding to different regions in which the sampling process is confined until the next region is discovered.

[i] A similar run with a knot 5_1 of length $N = 500$ has arrived to $m = 706$, suggesting that the highest energy value of a knot of a given length is dependent on its topology as intuitively expected.

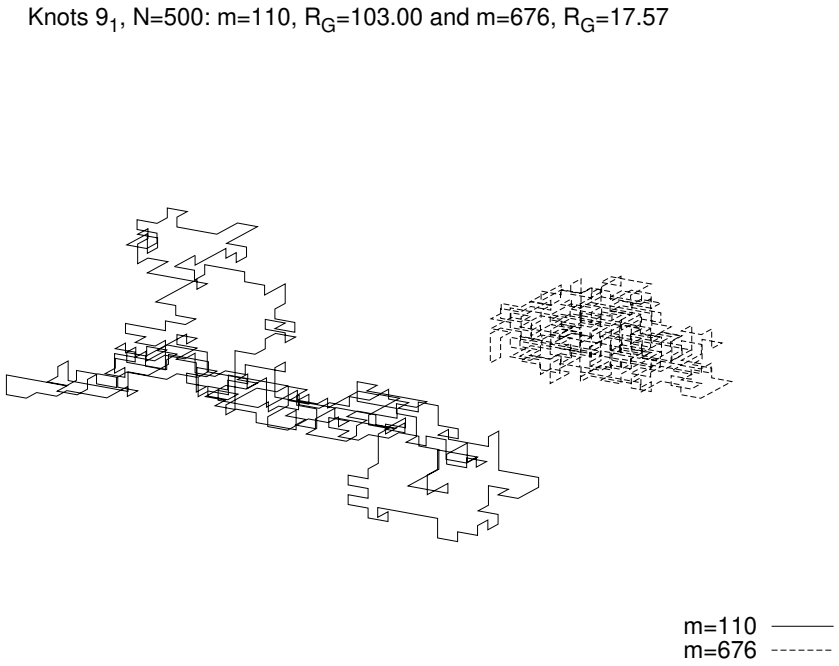

Fig. 17. The seed conformation (thin lines) is that of a knot 9_1 with $N = 500$, $m = 110$ and gyration radius $R_G \sim 107.00$ lattice units. The second conformation (thick lines) has been obtained by acting on the seed with random transformations. Its contact number and gyration radius (in lattice units) are given respectively by: $m = 676$ and $R_G \sim 17.57$. Both conformations are defined on a simple cubic lattice. In lattice units the seed knot roughly occupies a box of dimension $35 \times 30 \times 18$ while the second knot fits in a volume of dimensions $14 \times 10 \times 11$.

mean that the method of Ref. [56] is not consistent with the ergodicity of the system. Indeed, the pivot moves used here as random transformations are ergodic as shown in [31]. An entirely free knot would be able to avoid to get trapped within a narrow set of peculiar conformations by swelling. Unfortunately, this is prevented by the aforementioned compression condition. After relaxing this condition, still there is the problem that an enormous number of conformations must be sampled before the low energy spectrum characterized by compact conformations could be investigated. In fact, the knot must first swell starting from the initial conformation with $m = 101$ and then shrink again. The whole process needs a huge amount of time to take place, especially the spontaneous shrinking process. All these difficulties are absent when the topology is controlled with numerical knot invariants that allow arbitrarily large random transformations.

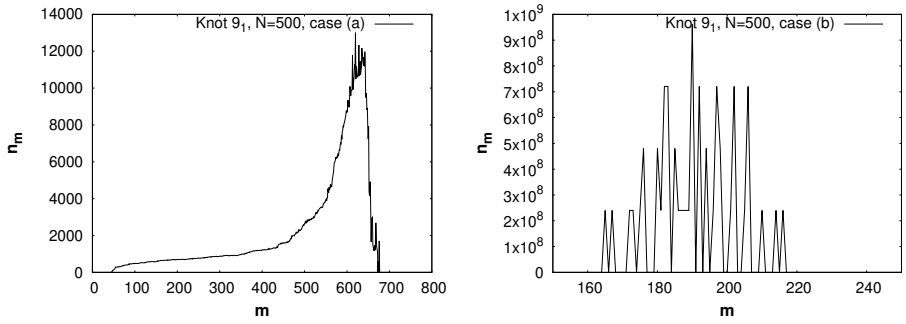

Fig. 18. Histograms plotting how many times n_m a conformation with contact number m has been visited while sampling the conformations of a knot 9_1 with $N = 500$ in order to explore the energy spectrum of this system. The histogram on the left − case (a) − has been obtained running a simulation in which the topology of the knot has been preserved using the Vassiliev knot invariant of degree 2. The other histogram − case (b) − has been produced following the method of Ref. [41]. In (a) a few millions of conformations span the wide energy range $45 \leq m \leq 676$. In (b) the system has been trapped in a limited set of conformations that have been visited billions of times.

8. Conclusions

In this work a comprehensive approach has been provided to implement numerical knot invariants (NKIs) in the study of knots formed by quasi one-dimensional physical objects like polymers rings or the lines of a magnetic field. The calculation of the contour integrals appearing in the expressions of NKIs has been tackled using the Monte Carlo algorithm summarised by Eqs. (3.14-3.17). In order to obtain the value of the NKIs the points of the knot are sampled via the three-step procedure whose details may be found on page 29. If knots are realized as a system of segments joined together to form a discrete loop, we have checked that the numerical evaluation of a NKI like the Vassiliev knot invariant of degree 2 is spoiled by the presence of the sharp corners appearing at the joints between continuous segments. spoils the numerical evaluation of NKIs. The departure from the exact result is roughly proportional to the number of sharp corners contained in the knot. In order to be able to apply NKIs in computer simulations, where knots are usually discrete objects, this difficulty has been solved introducing a fast and efficient procedure for smoothing knots. The idea followed in Section 4 is to substitute the parts of the knot in which there are sharp corners with smooth arcs. A family of smooth curves that are suitable for this goal has been given in parametric form in Eqs. (4.6–4.9). The arcs of these smooth curves are attached to the rest of the knot in such a way that the obtained new conformation is a closed G^1-curve. As a rule of thumb, the bigger are the portions of the knot around the sharp corners that are substituted, the faster is the calculation of the NKIs, see the comments in Point 4 on page 15. On the other side, if the smoothed region of the knot is too big, there is a high risk that the knot type could change. The size of these regions is determined by the lengths

d'_{i-1} and d_i, $i = 1, \ldots, N$, defined in Eqs. (4.4–4.5). In the case of knots on a lattice, it is possible to pick up a priori the values of d'_{i-1} and d_i in such a way that the topology of the knot is not affected by the smoothing procedure. The example of a simple cubic lattice has been worked out in Section 6, see Eqs. (6.1–6.3) and related comments. If however the segments of a discrete knot are allowed to get arbitrarily close to each other, as it happens when off-lattice computations are considered, a prescription to select the values of d'_{i-1} and d_i is needed. Such a prescription has been explained in details in Section 5. The basic strategy is to surround each joint in which there is a sharp corner with a sphere that contains the part to be changed and no other point of the knot. This and the additional condition that each sphere cannot have intersections with the other spheres are sufficient to prevent undesired topology changes. At the end, the values of d'_{i-1} and d_i are made to coincide with the radii of these spheres. The recursive presented in Section 5 is able to derive the radii of the spheres in such a way that both conditions mentioned above are respected. This procedure is relatively simple despite the fact that it is entirely general, being valid for knots both on- and off-lattice.

The algorithms developed in this work have been tested against concrete simulations whose aim is to determine the energy landscape of knotted polymer rings subjected to short-range attractive interactions. The Wang-Landau algorithm has been exploited as an engine for sweeping the set of all possible conformations and finding those with the lowest energy states. When the discrete knot to be investigated is very long, in the sense that it consists of many segments, this task is particularly demanding from the computational point of view independently of the method used in order to preserve their topology. The main reason is that the set of conformations of a discrete knot becomes soon huge when the number of segments N is increasing. To investigate a statistically relevant fraction of this set and succeed in picking up the rare conformations corresponding to the lowest energy states, a large number of conformations should be randomly generated. Our simulations have shown that the number of random transformations needed to explore the energy spectrum of knots including the most rare conformations is much lower if large parts of the knots are allowed to be changed. For instance, in the case of the knot 9_1 with $N = 500$ discussed in Section 7, a few millions of sampled conformations is sufficient to find the lowest energy state with $m = 576$. With the method of Ref. [56], in which the random transformations may involve at most four segments, hundreds of billions of conformations should instead be generated before arriving to a state with $m = 576$. A similar behaviour has been observed in the simulations of a knot 5_1 with $N = 500$ (the lowest energy state has contact number $m = 706$) and of a knot 4_1 with $N = 360$ (contact number of the lowest energy state: $m = 474$). The explanation of this fact is straightforward: In order to connect two conformations whose shapes are very different, many random transformations will be necessary if these transformations may affect only a tiny part of the knot. For this reason, algorithms for sampling knot conformations based on

NKIs to detect unwanted topology changes are very efficient in exploring the set of all conformations because in this way it is possible to perform random transformations of arbitrarily large elements of the knot. This advantage compensates the large number n of knot points that should be sampled according to Eq. (3.14) in order to compute the contour integrals appearing in the expressions of the NKIs. Moreover, thanks to the speeding up procedures explained in Section 6, together with a high degree of parallelisation and the use of GPUs, simulations in which n is in the average of the order of 10^8 become feasible. This high value of n is sufficient to treat knots with thousands of segments.

In conclusion, in this paper a comprehensive set of algorithms and techniques has been provided with the aim of implementing the application of NKIs in computer simulations involving discrete knots. The examples worked out in the case of the Vassiliev invariant of degree 2 have shown that NKIs allow to distinguish the topological states of discrete knots in an efficient and fast manner. The topology of knots like $3_1, 4_1, 5_1$ and 9_1 of different lengths up to $N = 500$ turns out to be preserved in all performed simulations after the generation of millions of random conformations. Work is in progress in order to extend these results also to the case of the triple invariant of Milnor that describes the links formed by three knots and several other invariants that have applications in various disciplines ranging from astrophysics to physics and chemistry [57,58,38].

Acknowledgments

The simulations reported in this work were performed in part using the HPC cluster HAL9000 of the Computing Centre of the Faculty of Mathematics and Physics at the University of Szczecin. The work of F. Ferrari and Y. Zhao results within the collaboration of the COST Action CA17139. The use of some of the facilities of the Laboratory of Polymer Physics of the University of Szczecin, financed by a grant of the European Regional Development Fund in the frame of the project eLBRUS (contract no. WND-RPZP.01.02.02-32-002/10) is gratefully acknowledged. F. Ferrari would like to thank Jarosław Paturej for fruitful discussions and for making available the GPUs on which part of the codes relevant to this paper have been run. Last but not last, both F. Ferrari and Y. Zhao are largely indebted to Christopher Westenberger for the help in tidying up some of the formulas in this paper and for pointing out Ref. [60].

Appendix A. Algorithm to find the point on a discrete knot that it is nearest to a given joint

Let $\boldsymbol{x}_{k+1,i}$ be the nearest point to the joint $\boldsymbol{x}_i$ among all points lying on the segment $\boldsymbol{l}_{k+1} = \boldsymbol{x}_{k+1} - \boldsymbol{x}_k$ with $k+1 \neq i-1, i$. To detect the position of $\boldsymbol{x}_{k+1,i}$, we pick up on $\boldsymbol{l}_{k+1}$ a general point $\boldsymbol{X}_{k+1}(\sigma)$ as follows:

$$\boldsymbol{X}_{k+1}(\sigma) = \boldsymbol{x}_k + (\boldsymbol{x}_{k+1} - \boldsymbol{x}_k)\sigma \tag{A.1}$$

with $\sigma \in [0,1]$. The distance between this point and $\boldsymbol{x}_i$ is $\sqrt{(\boldsymbol{X}_{k+1}(\sigma)-\boldsymbol{x}_i)^2}$. If $\boldsymbol{X}_{k+1}(\sigma)$ is the position of the nearest point to $\boldsymbol{x}_i$, then $\boldsymbol{X}_{k+1}(\sigma)$ must satisfy the condition

$$\frac{d\sqrt{(\boldsymbol{X}_{k+1}(\sigma)-\boldsymbol{x}_i)^2}}{d\sigma}=0 \tag{A.2}$$

Inserting Eq. (A.1) in (A.2) and solving Eq. (A.2) with respect to σ, we obtain that the point of $\boldsymbol{l}_{k+1}$ at the minimal distance from $\boldsymbol{x}_i$ corresponds to the following value of σ:

$$\sigma_{\min}=-\frac{(\boldsymbol{x}_{k+1}-\boldsymbol{x}_k)\cdot(\boldsymbol{x}_k-\boldsymbol{x}_i)}{(\boldsymbol{x}_{k+1}-\boldsymbol{x}_k)^2} \tag{A.3}$$

Three cases may occur:

1) If $\sigma_{\min}\geq 1$, the nearest point to $\boldsymbol{x}_i$ clearly lies outside the segment $\boldsymbol{l}_{k+1}$, because the points of $\boldsymbol{l}_{k+1}$ are in the interval $\sigma\in[0,1]$. The fact that σ_{min} is positive tells us that going along $\boldsymbol{l}_{k+1}$ in the direction pointing toward the end point $\boldsymbol{x}_{k+1}$ we are increasingly getting closer to the point $\boldsymbol{x}_i$. Continuing in the same direction, the nearest point to $\boldsymbol{x}_i$ occurs to be at the distance $\sigma_{\min}$ from the point $\boldsymbol{x}_k$. Since $\sigma_{\min}>1$, this point is outside the segment $\boldsymbol{l}_{k+1}$. In conclusion, the nearest point to $\boldsymbol{x}_i$ lying on the segment $\boldsymbol{l}_{k+1}$ is $\boldsymbol{x}_{k+1,i}=\boldsymbol{x}_{k+1}$ and its distance from $\boldsymbol{x}_i$ is $d_{k+1,i}=|\boldsymbol{x}_{k+1}-\boldsymbol{x}_i|$.
2) If $\sigma_{\min}\leq 0$, the nearest point occurs as before outside the segment $\boldsymbol{l}_{k+1}$. Moreover, the fact that $\sigma_{\min}$ is negative implies that the point $\boldsymbol{x}_i$ is closer to the end $\boldsymbol{x}_k$ of $\boldsymbol{l}_{k+1}$ than to any other point of $\boldsymbol{l}_{k+1}$. As a consequence, on the segment $\boldsymbol{l}_{k+1}$, the nearest point to $\boldsymbol{x}_i$ is in this case the point $\boldsymbol{x}_k$. Its distance from $\boldsymbol{x}_i$ is $d_{k+1,i}=|\boldsymbol{x}_k-\boldsymbol{x}_i|$.
3) If $0<\sigma_{\min}<1$, then $\boldsymbol{x}_{k+1,i}$ lies on the segment $\boldsymbol{l}_{k+1}$ and $\boldsymbol{x}_{k+1,i}=\boldsymbol{x}_{k+1}+(\boldsymbol{x}_{k+1}-\boldsymbol{x}_k)\sigma_{\min}$. The distance of $\boldsymbol{x}_{k+1,i}$ from $\boldsymbol{x}_i$ is in this case:

$$d_{k+1,i}=\sqrt{(\boldsymbol{x}_k-\boldsymbol{x}_i)^2-\frac{\left[(\boldsymbol{x}_{k+1}-\boldsymbol{x}_k)\cdot(\boldsymbol{x}_k-\boldsymbol{x}_i)\right]^2}{(\boldsymbol{x}_{k+1}-\boldsymbol{x}_k)^2}} \tag{A.4}$$

By repeating this procedure for all segments $\boldsymbol{l}_{k+1}$ with $k=0,\cdots,N-1$ and $k\neq i-1,i$, we obtain the location of the point of the knot which is not belonging to $\boldsymbol{l}_i$ and $\boldsymbol{l}_{i+1}$, and it is nearest to $\boldsymbol{x}_i$.

References

[1] S. A. Wasserman and N. R. Cozzarelli, Biochemical topology: applications to DNA recombination and replication. Science 232 (1986), 951-960.
[2] M. Delbrück and F. Brock-Füller: Mathematical Problems in the Biological Sciences in: E. R. Bellman (Ed.), Proc. Symp. Appl. Math. 14, Providence, RI: American Mathematical Society (1962), 55.
[3] M. J. Bowick, L. Chander, E. A. Schiff and A. M. Srivastava.: it The Cosmological Kibble Mechanism in the Laboratory: String Formation in Liquid Crystals, Science 263 (1994), 943-945.

[4] C. Bäuerle, Yu. M. Bunkov, S. N. Fisher, H. Godfrin and G. R. Pickett, Laboratory simulation of cosmic string formation in the early Universe using superfluid ^{3}He, Nature 382 (1996), 332-334.
[5] V. M. H. Ruutu, V. B. Eltsov, A. J. Gill, T. W. B. Kibble, M. Krusius, Yu. G. Makhlin, B. Placais, G. E. Volovik and W. Xu, Vortex formation in neutron-irradiated superfluid ^{3}He as an analogue of cosmological defect formation, Nature 382 (1996), 334-336.
[6] T. Araki and H. Tanaka, Colloidal Aggregation in a Nematic Liquid Crystal: Topological Arrest of Particles by a Single-Stroke Disclination Line, Phys. Rev. Lett. 97 (2006), 127801-4.
[7] U. Tkalec, M. Ravnik, S. Čopar, S. Žumer and I. Muševič, Reconfigurable Knots and Links in Chiral Nematic Colloids, Science 333 (2011), 62-65.
[8] S. Žumer: 21st International Liquid Crystal Conference, Keystone, Colorado, USA, July 2-7, 2006, Kinsley & Associates, Littletown, (2006).
[9] J. W. Alexander, Topological Invariants of Knots and Links, Trans. Amer. Math. Soc. 30 (1928), 275-306.
[10] L. H. Kauffman, Knots and Physics, 2nd ed., World Scientific, Singapore, (2001).
[11] P. Freyd, D. Yetter, J. Hoste, W. B. R. Lickorish, K. Millet and A. Ocneanu, A new polynomial invariant of knots and links, Bull. AMS 12 (1985), 239-246.
[12] M. Kontsevich, Vassiliev's knot invariants, Preprint, Max-Planck-Institut für Mathematik, Bonn.
[13] D. Bar-Natan, On the Vassiliev knot invariants, Harvard preprint (1992).
[14] D. Bar-Natan, On the Vassiliev Knot Invariants, Topology 34 (1995), 423-472.
[15] J. M. F. Labastida and A. V. Ramallo, Operator formalism for Chern-Simons theories, Phys. Lett. B 227 (1989), 92-102.
[16] E. Guadagnini, M. Martellini and M. Mintchev, Braids and quantum group symmetry in Chern-Simons theory, Nucl. Phys. B 336 (1990), 581-609.
[17] M. Alvarez and J. M. F. Labastida, Nucl.Phys. B433 (1995), 555-596; Erratum-ibid. B441 (1995), 403-404.
[18] A. V. Vologodskii, A. V. Lukashin, M. D. Frank-Kamenetskii and V. V. Anshelevich, The knot problem in statistical mechanics of polymer chains, Zh. Eksp. Teor. Fiz. 66 (1974), 2153-2163.
[19] T. T. F. Nonweiler, The Numerical Evaluation of Curvilinear Integrals and Areas Defined by Discrete Data, Inter-university/research councils series (1972).
[20] P. Davis and P. Rabinowitz, Methods of Numerical Integration, 2nd Ed, New York, Academic Press (1984).
[21] K. Atkinson and E. Venturino, Numerical Evaluation of Line Integrals, Siam J. Numer. Anal. 30 (1993), 882-888.
[22] C. Perego and R. Potestio, Journal of Physics: Condensed Matter, 31 (2019), 443001.
[23] L. Tubiana, G. Polles, E. Orlandini et al., KymoKnot: A web server and software package to identify and locate knots in trajectories of linear or circular polymers, Eur. Phys. J. E 41 (2018), 72.
[24] C. Micheletti, D. Marenduzzo, E. Orlandini and D. W. Sumners, Knotting of random ring polymers in confined spaces, Journal of Chemical Physics 124 (6) (2006), 64903–64903.
[25] M. Baiesi, E. Orlandini and A. L. Stella, Ranking Knots of Random, Globular Polymer Rings, Phys. Rev. Lett. 99 (2007), 058301–058301.
[26] M. Baiesi, E. Orlandini and S. G. Whittington, Interplay between writhe and knotting for swollen and compact polymers, Journal of Chemical Physics 131 (15) (2009), 154902.
[27] G. D. Knott, Interpolating Cubic Splines, Boston, Birkhäuser (2000).

[28] P. Dunin-Barkowski, A. Sleptsov and A. Smirnov, Kontsevich integral for knots and Vassiliev invariants, Int. J. Mod. Phys. A 28 (2013), 1330025-62.
[29] Y. Zhao and F. Ferrari, A study of polymer knots using a simple knot invariant consisting of multiple contour integrals, JSTAT 2013 (2013), P10010.
[30] P. J. Davis and P. Rabinowitz, Methods of numerical integration, Boston, MA, Academic Press, (1984).
[31] N. Madras, A. Orlitsky and L. A. Sepp, Monte Carlo Generation of Self-Avoiding Walks with Fixed Endpoints and Fixed Length, J. Stat. Phys. 38 (1990), 159-183.
[32] N. Lesh, M. Mitzenmacher and S. Whitesides, A Complete and Effective Move Set for Simplified Protein Folding, Proceedings of the Seventh Annual International Conference on Research in Computational Molecular Biology (RECOMB-03), 188-195 (2003).
[33] C. Aragão de Carvalho, S. Caracciolo and J. Fröhlich, Polymers and g$|\phi|^4$ theory in four dimensions, Nucl. Phys. B 215 (1983), 209.
[34] B. Berg and D. Foerster, Random paths and random surfaces on a digital computer, Phys. Lett. B 106 (1981), 323.
[35] E. Witten, Quantum field theory and the Jones polynomial, Commun. Math. Phys. 121 (1989), 351-399.
[36] A. S. Cattaneo, P. Cotta-Ramusino and M. Martellini, Three-dimensional BF theories and the Alexander-Conway invariant of knots, Nucl. Phys. B 436 (1-2) (1995), 355-382.
[37] M. Polyak and O. Viro, On the Casson knot invariant, J. Knot Theory Ramifications 10 (2001), 711-738.
[38] F. Ferrari, A new strategy to microscopic modeling of topological entanglement in polymers based on field theory, Nucl. Phys. 948 (2019), 114778.
[39] H. Kleinert, Path Integrals in Quantum Mechanics, Statistics, Polymer Physics, and Financial Markets, (World Scientific Publishing, 3rd Ed., Singapore, 2003).
[40] L. Qu and D. He, Solving Numerical Integration by Particle Swarm Optimization, Work published in the Proceedings of ICICA 2010, Part II, Zhu, R. et Al. (Eds), Berlin, Heidelberg, Springer Verlag, 228-235 (2010).
[41] K. Koniaris and M. Muthukumar, Knottedness in ring polymers, Phys. Rev. Lett. 66 (1991), 2211-2214.
[42] W. R. Taylor and A. Aszódi, Protein Geometry, Classification, Topology and Symmetry: A Computational Analysis of Structure, New York, Taylor & Francis Group, (2005).
[43] L. F. Liu, J. L. Davis and R. Calendar, Novel topologically knotted DNA from bacteriophage P4 capsids: studies with DNA topoisomerases, Nucleic Acids Res. 9 (1981), 3979-3989.
[44] L. F. Liu, L. Perkocha, R. Calendar and J. C. Wang, Knotted DNA from bacteriophage capsids, Proc. Natl. Acad. Sci. USA 78 (1981), 5498-5502.
[45] J. Arsuaga, M. Vazquez, S. Tigueros, D. W. Sumners and J. Roca, Knotting probability of DNA molecules confined in restricted volumes: DNA knotting in phage capsids, Proc. Natl. Acad. Sci. USA 99 (2002), 5373-5377.
[46] E. J. van Rensburg, and S. Whittington, The knot probability in lattice polygons, J. Phys. A Math. Gen. 23 (1990), 3573-3590.
[47] R. Metzler, T. Ambiörsson,, A. Hanke, Y. Zhang, S. Levene, Single DNA Conformations and Biological Function, Jour. Comput. Teor. Nanoscience 4 (1) (2007), 1.
[48] D. Kleckner, L. H. Kauffman and W. T. M. Irvine, How superfluid vortex knots untie, Nature Physics 12 (2016), 650.
[49] M. Berger and M. Asgari-Targhi, Self-organized braiding and the structure of coronal loops, APJ 705 (2009), 347.

[50] T. Stauch, A. Dreuw, Knots "Choke Off" Polymers upon Stretching, Angewandte Chemie (Int. Ed.), 55 (2) (2016), 811.
[51] D. A. Leigh, L. Pirvu and F. Schaufelberger, Stereoselective synthesis of molecular square and granny knots, J. Am. Chem. Soc. 141 (14) (2019), 6054.
[52] M. Doi and S. F. Edwards, The Theory of Polymer Dynamics, Clarendon Press (1988).
[53] M. Rubinstein and R. H. Colby, Polymer Physics, Oxford University Press (2003), ISBN: 019852059X.
[54] F. Wang and D. P. Landau, Efficient, multiple-range random walk algorithm to calculate the density of states, Phys. Rev. Lett. 86 (10) (2001), 2050.
[55] P. N. Vorontsov-Velyaminov, N. A. Volkov and A. A. Yurchenko, Entropic sampling of simple polymer models within Wang–Landau algorithm, J. Phys. A: Math. Gen. 37 (5), 1573-1588 (2004).
[56] Y. Zhao and F. Ferrari, A numerical technique for studying topological effects on the thermal properties of knotted polymer rings, JSTAT J. Stat. Mech. (2012), P11022.
[57] F. Ferrari, Topological field theories with non-semisimple gauge group of symmetry and engineering of topological invariants, rozdział, in Current Topics in Quantum Field Theory Research, O. Kovras (Ed.), Nova Science Publishers (2006), ISBN: 1-60021-283-2.
[58] F. Ferrari, M. R. Piatek and Y. Zhao, A topological field theory for Milnor's triple linking number, J. Phys. A: Mathematical and Theoretical, 48 (2015), 275402, arXiv: 1411.6429.
[59] Y. He, X. F. Gu and H. Qin, Automatic Shape Control of Triangular B-Splines of Arbitrary Topology, Jour. Comput. Sci. & Technol. 21 (2006), 232-237.
[60] C. Westenberger, Knots and links from random projections, arXiv preprint arXiv:1602.01484 (2016).